Brigham Young University
BYU ScholarsArchive

All Theses and Dissertations

2007-03-16

On-Chip Atomic Spectroscopy

Donald B. Conkey
Brigham Young University - Provo

Follow this and additional works at: https://scholarsarchive.byu.edu/etd

 Part of the Electrical and Computer Engineering Commons

BYU ScholarsArchive Citation

Conkey, Donald B., "On-Chip Atomic Spectroscopy" (2007). *All Theses and Dissertations*. 858.
https://scholarsarchive.byu.edu/etd/858

This Thesis is brought to you for free and open access by BYU ScholarsArchive. It has been accepted for inclusion in All Theses and Dissertations by an authorized administrator of BYU ScholarsArchive. For more information, please contact scholarsarchive@byu.edu, ellen_amatangelo@byu.edu.

ON-CHIP ATOMIC SPECTROSCOPY

by

Donald B. Conkey

A thesis submitted to the faculty of

Brigham Young University

in partial fulfillment of the requirements for the degree of

Master of Science

Department of Electrical and Computer Engineering

Brigham Young University

April 2007

BRIGHAM YOUNG UNIVERSITY

GRADUATE COMMITTEE APPROVAL

of a thesis submitted by

Donald B. Conkey

This thesis has been read by each member of the following graduate committee and by majority vote has been found to be satisfactory.

Date	Aaron R. Hawkins, Chair
Date	Stephen M. Schultz
Date	Richard. H. Selfridge

BRIGHAM YOUNG UNIVERSITY

As chair of the candidate's graduate committee, I have read the thesis of Donald B. Conkey in its final form and have found that (1) its format, citations, and bibliographical style are consistent and acceptable and fulfill university and department style requirements; (2) its illustrative materials including figures, tables, and charts are in place; and (3) the final manuscript is satisfactory to the graduate committee and is ready for submission to the university library.

Date	Aaron R. Hawkins Chair, Graduate Committee

Accepted for the Department

Date	Michael J. Wirthlin Graduate Coordinator

Accepted for the College

Date	Alan R. Parkinson Dean, Ira A. Fulton College of Engineering and Technology

ABSTRACT

ON-CHIP ATOMIC SPECTROSCOPY

Donald B. Conkey

Department of Electrical and Computer Engineering

Master of Science

This thesis presents the integration of atomic vapor cells with anti-resonant reflecting optical waveguides (ARROWs) fabricated on silicon chips. These potentially provide a compact platform for a number of optical applications, including the study of quantum coherence effects such as electromagnetically induced transparency and single-photon nonlinearities, as well as frequency stabilization standards. The use of hollow waveguides allows for light propagation in low index (vapor) media with compact mode areas. ARROWs make particularly attractive waveguides for this purpose because they can be interfaced with solid core waveguides, microfabricated on a planar substrate, and are effectively single mode. ARROW fabrication utilizes an acid-removed sacrificial core surrounded by alternating plasma deposited dielectric layers, which act as Fabry-Perot reflectors.

To demonstrate the effectiveness of the ARROW as a vapor cell, a platform consisting of solid and hollow core waveguides integrated with rubidium vapor cells was developed. A variety of sealing techniques were tested for vapor cell integration with the ARROW chip and for compatibility with rubidium. Rubidium was used because it is of particular interest for studying quantum coherence effects. Liquefied rubidium was transferred from a bulk supply into an on-chip vapor cell in an anaerobic atmosphere glovebox. Optical absorption measurements confirmed the presence of rubidium vapor within the hollow waveguide platform. Further analysis of the measurements revealed high optical density of rubidium atoms in the hollow core. Saturated absorption spectroscopy measurements verified that the on-chip integrated vapor cell was suitable for common precision spectroscopy applications.

ACKNOWLEDGMENTS

I am grateful to the individuals who have supported me throughout the preparation of this thesis. Foremost I would like to thank Dr. Hawkins for providing me with this research opportunity and for continual support throughout my undergraduate and graduate years. I would also like to thank John Barber, who trained me in many microfabrication techniques essential to the fabrication of ARROWs. Thanks to our collaborators at the University of California at Santa Cruz, Dr. Schmidt, Wenge Yang, and Bin Wu, who have provided excellent optical measurements, device characterizations and insights. Special thanks to John Hulbert and Becky Brenning for aiding me with the tedious testing and fabrication of vapor cells. I am indebted to Evan Lunt and Brian Phillips who have helped me with the ARROW fabrication process and have finished devices for me when I was not physically able. I would especially like to thank my best friend and wife, Emily, for all the love and encouragement she has given me.

TABLE OF CONTENTS

LIST OF TABLES

LIST OF FIGURES

1 Introduction

1.1 Overview

Large vapor cells are used to investigate a variety of quantum interference effects. Atomic clocks [1], nonlinear frequency generation [2], gas phase sensing [3], precision spectroscopy [3, 4], low-level switching [5], and the use of electromagnetically induced transparency [6] in slow light [7, 8], and quantum communications [9] are many of the effects that can be observed when light interacts with atomic vapor in these cells. In these conventional bulk vapor cells there is a tradeoff between small beam areas and finite focal depth. Hollow waveguides decouple this tradeoff and allow for long intensities over large distances. This long interaction length with the atomic vapor makes hollow waveguides ideal platforms for observation of quantum interference effects. Many gases and molecular vapors can be optically investigated, but alkali vapors are of particular interest for quantum interference effects.

On chip vapor cells would miniaturize and simplify the measurement apparatus used to observe the aforementioned effects. Several miniaturized cells already exist: the NIST miniature vapor cell [1, 10] and photonic bandgap fibers have been integrated with rubidium vapor [2]. In this thesis a platform based on hollow anti-resonant reflecting optical waveguides (ARROWs) integrated with atomic vapor cells is described. ARROWs coupled with solid-core waveguides for off-chip fiber optical access form

monolithically integrated chips. With a footprint of less than 1 cm^2 and a cell volume over seven orders of magnitude smaller than bulk cells, ARROW chips are very small. ARROWs also have a micron sized mode area, which enables high intensities over near centimeter lengths on chip.

This thesis discusses the effectiveness of hollow core ARROWs for use as an integrated vapor cell platform, specifically for absorption spectroscopy applications. The introduction chapter provides background information about absorption spectroscopy, saturation absorption spectroscopy, and some current apparatuses for investigating photon-atom interactions. These other apparatuses include atomic vapor cells, the NIST cell, and photonic band-gap fibers. Chapter Three briefly discusses ARROW principles and fabrication techniques. The benefits of using ARROWs as integrated vapor cells are also described. Chapter Four explains how the ARROW is modified to contain atomic vapor. Chapter Five presents optical measurements and certain characteristics of the rubidium vapor in the hollow core waveguide.

The measurements show the effectiveness of sealing techniques and transferring rubidium atoms through a hollow channel. Absorption spectroscopy measurements of rubidium vapor in the hollow core ARROW, as well as optical density measurements of rubidium in an ARROW show the effectiveness of photon-atom interactions in the hollow core. The advantages of the planar integration of a vapor cell are shown with a scattering measurement. Finally, saturation absorption spectroscopy is demonstrated. All of these demonstrate that an ARROW device satisfies key requirements for integrated atomic spectroscopy.

1.2 Contributions

The research presented in this thesis represents a collaborative effort with the University of California at Santa Cruz (UCSC). My responsibility has been the design, development, and integration of vapor cells with the ARROW waveguide. Fabrication of the ARROW waveguides for integration with vapor cells was also performed by me in the BYU Integrated Microfabrication Laboratory (IML). UCSC performed the optical design and testing of the ARROWs, as well as the testing of the integrated ARROW vapor cells. This thesis focuses on the integration of the ARROW device for atomic spectroscopy. Significant optical test results from UCSC are included, as they show the performance of the integrated vapor cell.

This research provides a unique contribution to integrated optics and atomic spectroscopy. From this research two peer-reviewed journal articles have been published [11,12], with another currently being reviewed [13] and five conference presentations have been given [14-18], including an invited talk [18]. These papers and presentations and this thesis lay the foundation for the work to come in utilizing the full-potential of the ARROW as a platform for atomic spectroscopy and quantum interference effects.

2 Atomic Spectroscopy

2.1 Absorption Spectroscopy

As electromagnetic energy from a laser beam propagates through a sample of atomic vapor, atoms absorb the energy from the photons. Consequently, the photons which lose their energy to the atomic vapor are not detected in the output. The resulting output spectrum contains dips around the frequencies of the absorbed photons (Figure 2.2). These frequencies reveal the atomic energy structure of the atom and the density of the atoms in the sample. The relative intensity of the transmitted light varies proportionally to the molar concentration of the vapor and the thickness of the sample. These can be determined by the Beer-Lambert Law:

$$I_1 = I_0 * \exp(-\alpha * L). \quad (1)$$

I_1 and I_0 are the resulting and incident intensities. α is the absorption coefficient, which depends on the density of atoms. L is the path length of the light through the atomic vapor.

Absorption spectroscopy for alkali atoms is best explained in a simple hydrogen-like atomic energy level scheme. Alkali atoms have the same outer electronic configuration as hydrogen. The inner shells of alkali atoms are all full of electrons and closed, therefore they can be neglected. The outer, valence shell only has one electron,

like hydrogen. Without the presence of an external field the valence electron will stay at its lowest energy level, which is referred to as the ground state. This is ideal, because when there are an equal number of atoms in both excited and ground states, photons are as likely to be spontaneously emitted as absorbed. The laser signal would not attenuate and yield any dips in its transmission in this case. The attenuation of the signal can be maximized when all atoms are in the ground state.

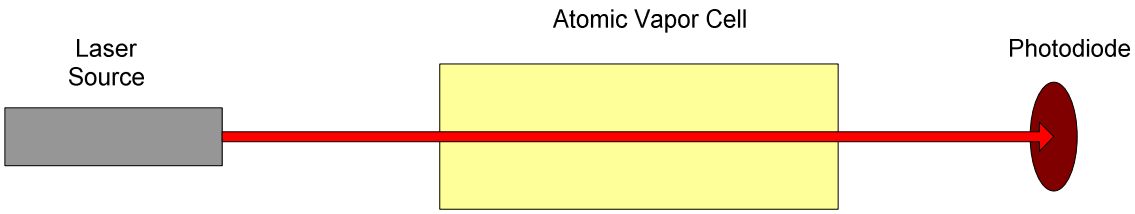

Figure 2. 1 Basic setup for absorption spectroscopy.

To measure an absorption spectrum, the simple configuration shown in Figure 2.1 is used. The atomic vapor cell would be full of whichever atoms are to be analyzed. A laser would be selected that could scan through the natural frequency of the atoms. When the transmission spectrum is observed, there is a smooth absorption curve around the true natural absorption frequency. Figure 2.2 shows a sample absorption plot from rubidium. The four dips are from four separate energy transitions and will be explained later. Each dip spreads out in a Gaussian curve due to thermal motions in individual atoms in the gas. If an atom is moving toward the beam the frequency from the perspective of the atom is red-shifted. Thus, it will absorb light at a frequency less than the natural frequency of the atom. The same is true for atoms moving away from the beam, although they blue-shift the frequency. These cause absorption in a wider spectrum than just the natural

frequency. This is referred to as Doppler broadening. It does not pose a problem when looking at absorption dips several nanometers apart.

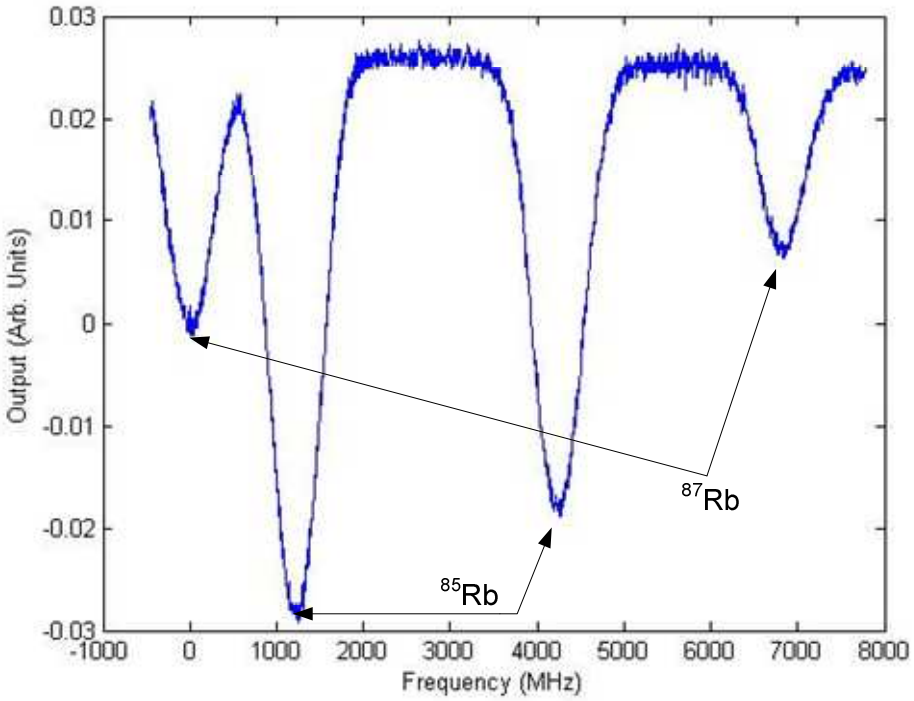

Figure 2. 2 The absorption spectrum of rubidium's two natural isotopes around the D_2 transition. Frequency is labeled to show the frequency difference between the dips, with the first dip used as a reference.

2.2 Atomic Energy Level Splitting

Energy levels are split in two ways, fine and hyperfine splitting. The first, fine splitting, comes about through an electromagnetic interaction between an electron and its nucleus. From the electrons perspective, the nucleus spins around it. This sets up a magnetic field which interacts with the magnetic moment of the electron, thus altering its energy. The energy changes based on the orientation of the electrons spin relative to the angular momentum of the orbit. The difference of wavelengths from fine splitting is

typically on the order of nanometers. Figure 2.3 shows the few lowest energy levels of rubidium. The first excited energy state is fine split into two energy levels: $5^2P_{1/2}$ and $5^2P_{3/2,}$ with a 15 nm difference in wavelength. The rubidium energy level structure will be discussed further in the next section.

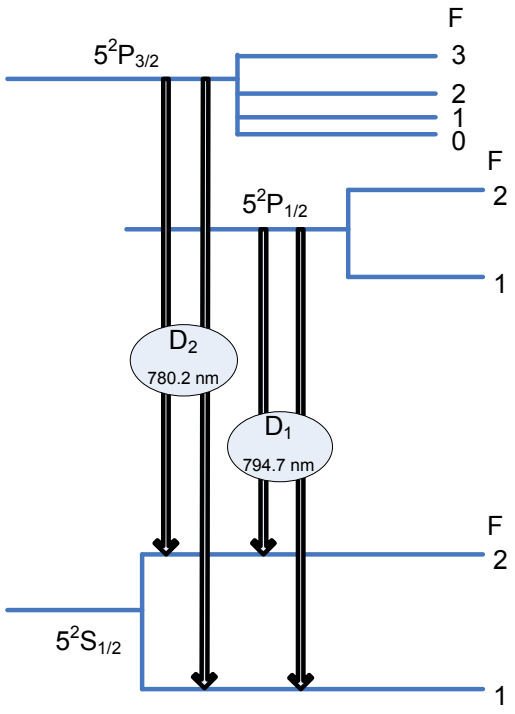

Figure 2. 3 The energy structure of rubidium showing its few lowest energy levels.

Hyperfine splitting is the second way in which energy levels split. The magnetic moment of the valence electron changes as it interacts with the magnetic moment of the nucleus. The hyperfine splitting comes from the difference in energy of the orientations of the magnetic dipoles. It is characterized by the angular momentum quantum number F. Figure 2.3 shows how $5^2S_{1/2}$ and $5^2P_{1/2}$ are split into two, and $5^2P_{3/2}$ is split four hyperfine levels. As the name suggests, hyperfine splitting is on a much smaller scale than fine splitting, 10^{-3} nm. In fact, it is smaller than the Doppler broadened spectrum of a single

line. This means that, because of Doppler broadening, absorption spectroscopy does not have high enough resolution to show the hyperfine levels. Therefore, special means, such as saturated absorption spectroscopy, are required to observe the hyperfine splitting of atomic energy levels.

2.3 Rubidium Energy Structure

Rubidium is commonly used for investigation of atomic energy levels. Rubidium is an alkali atom and has all the benefits of the hydrogen-like structure alkali atoms possess as discussed in the previous section. It also has natural absorption wavelengths around 780 nm, which is a wavelength of readily available lasers. Also, much noteworthy research on quantum interference has been done using it [19]. Furthermore, rubidium provides a wavelength reference and a three level energy scheme used for many quantum interference effects [19, 20]. These characteristics make rubidium highly used in slow light research as well [19].

The ground state of rubidium, denoted $5^2S_{1/2}$ contains one valence electron. It is also split into two hyperfine sublevels (Figure 2.4). The first excited state of rubidium is also split, but is characterized by a fine split. These two states are denoted $5^2P_{1/2}$ and $5^2P_{3/2,}$ and are separated by 15 nm in wavelength. The transitions that may take place as electromagnetic energy interacts with the atoms are denoted D_1 and D_2 (Figures 2.3). The D_1 transition corresponds to a 795 nm wavelength and represents the transition between the $5^2S_{1/2}$ and the lower energy excited state $5^2P_{1/2}$. The D_2 transition corresponds to the transition between $5^2S_{1/2}$ to the higher energy excited state $5^2P_{3/2,}$ and has a wavelength of 780 nm.

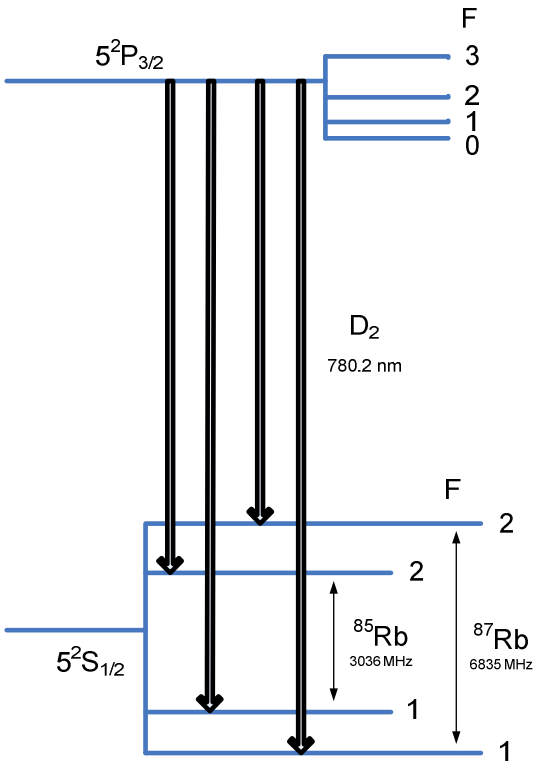

Figure 2. 4 The difference in the split ground state energy level of rubidium's natural isotopes. These transitions correspond to the absorption peaks in Figure 2.2.

Another reason rubidium is good for absorption spectroscopy is its two naturally occurring isotopes, which are both in reasonable abundance. Rubidium 85 is at 72 percent abundance, and rubidium 87 takes in the other 28 percent. This is advantageous because it means that there are actually four groups of transitions, a D_1 and D_2 transition for both ^{85}Rb and ^{87}Rb. Figure 2.4 shows how the hyperfine splitting of the ground state differs between isotopes. All of the transitions represented in Figure 2.4 can be seen in the absorption spectrum plot in Figure 2.2. Notice how the frequency difference between dips corresponds to the frequency difference shown in Figure 2.5. Also, notice how the more abundant rubidium 85 absorbs more light than rubidium 87.

2.4 Saturated Absorption Spectroscopy

A second laser beam propagating through and saturating the atomic transitions reveals the hyperfine structure of atoms. This second beam has the same frequency as the first, because it comes from the same source. However, it has a different intensity and propagates through the atomic vapor in the opposite direction. Figure 2.5 shows a setup used for saturated absorption spectroscopy. The more intense saturation beam excites the atoms to an excited state. Due to the fast rate of emission and absorption transitions the strong resonant laser field causes the ground state and the excited state populations to equilibrate. This effectively saturates the transition. The less intense probe beam does not have many atoms available to excite, because the saturation beam has already excited them. This leaves transmission dips in the absorption peaks called Lamb dips. Each Lamb dip corresponds to a hyperfine energy transition. Figure 2.6 shows the possible hyperfine energy transitions possible in rubidium vapor. Figure 2.7 shows a saturated absorption spectrum of the D_2 transition in rubidium. Notice how the absorption dip has two Lamb dips, each corresponding to an allowed energy transitions of rubidium shown in Figure 2.6.

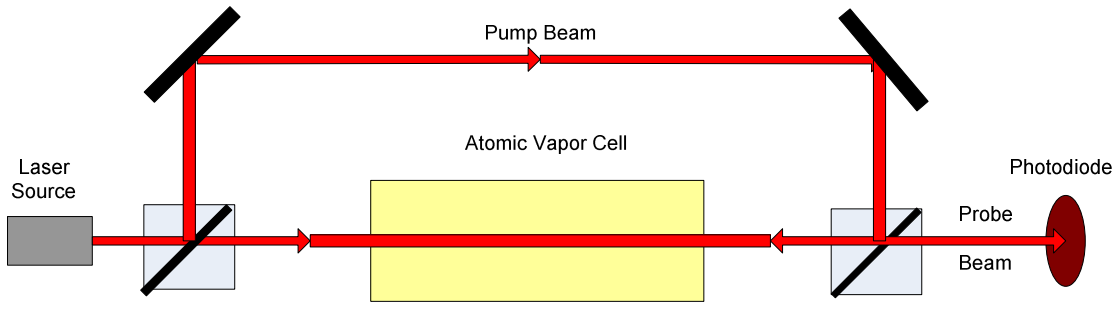

Figure 2. 5 Saturation absorption spectroscopy setup.

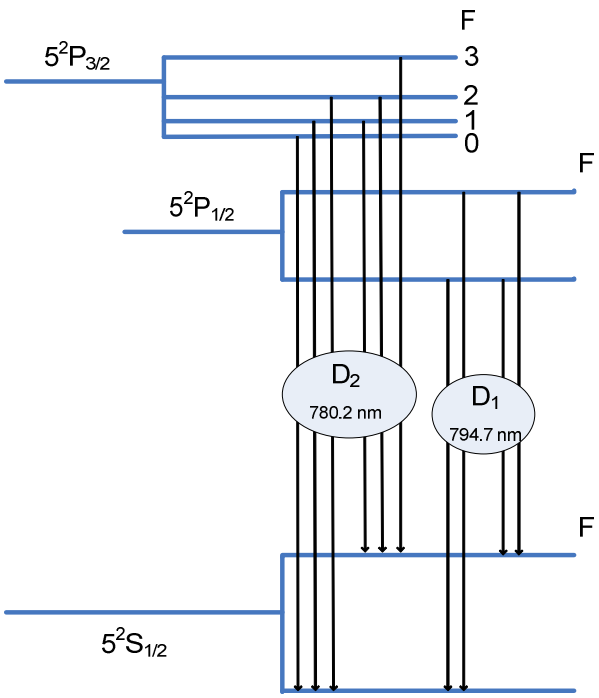

Figure 2. 6 The energy structure of rubidium, detailing its hyperfine transitions.

A key element to saturated absorption spectroscopy is tuning the frequency to the center of the natural frequency. If the lasers are not tuned to the center, both beams will be absorbed. The saturation beam will have no effect on the probe beam, because the two beams have excited different atoms in the Doppler profile. For example, if the laser wavelength is less than the center of the absorption peak, the saturation beam only excites atoms moving toward the beam with some velocity. From the atoms perspective the wavelength of the beam is actually at its resonant frequency, because the velocity red shifted the beam's frequency. At the same time the probe beam propagates in the opposite direction. The probe beam can only excite atoms moving with the same velocity in the opposite direction, because of the Doppler shift and the opposite propagation direction. Both of the beams have affected different atoms. The laser wavelength must be exactly at the transition frequency to observe increased transmission in the probe beam.

The probe beams Lamb result completely from atoms with zero velocity. Therefore, the linewidth of Lamb dips is not determined by Doppler broadening, but by the transition. This allows greater resolution and the small hyperfine transitions to be seen. Scanning through the natural frequency allows the absorption dips and the Lamb dips to be shown (Figure 2.7).

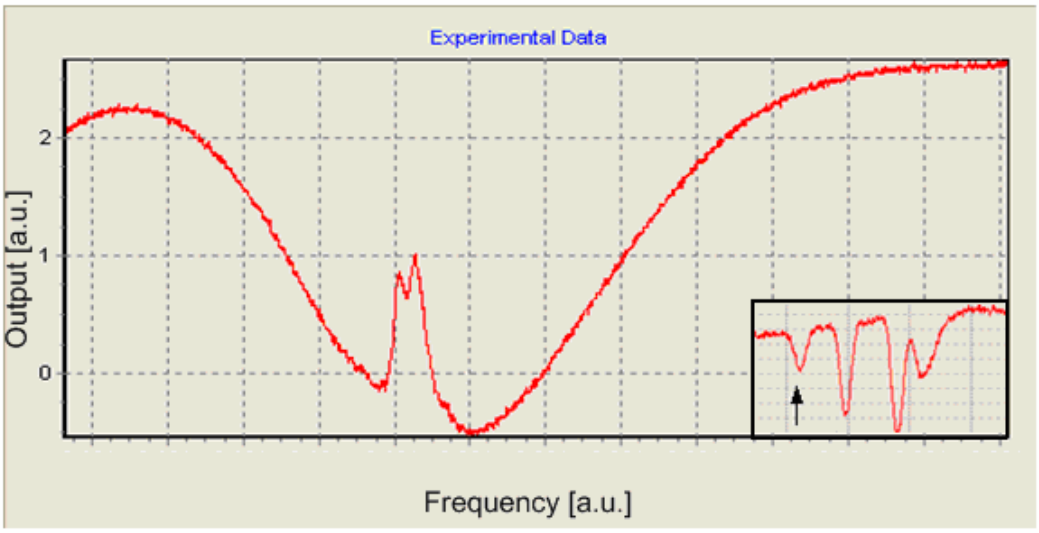

Figure 2. 7 The saturation absorption spectrum of a D_2 transition in ^{87}Rb showing two Lamb dips.

2.5 Atomic Vapor Cells

Atomic vapor cells are the primary source for atomic vapors used in alkali vapor absorption spectroscopy and other photon-atom interaction processes. These cells have been used for these measurements for several decades. In fact, the fabrication of the cells has not changed very much since Bouchiat and Brossel started applying coatings to cells in 1966 [21-23]. The coatings prevent the alkali atoms in the cell from adsorbing onto the surface of the glass walls [21]. This allows for more atoms to be in the optical beam path.

The coated walls also help the atoms maintain phase coherence despite atom-wall collisions, which is essential to produce many quantum optical effects.

Fabricating conventional atomic vapor cells requires a complex system of glassware attached to a bulk rubidium ampoule, a vacuum, several valves, and the cell. Glassblowers typically form this complex apparatus. To coat the cells a rod with paraffin flakes is inserted into the cell and the cell is vacuumed out. The rod is within the glass pipe network and does not affect the vacuum. Then, in an oven, the temperature is increased to evaporate the paraffin onto the walls. Following the rod's removal from the cell, rubidium is moved toward the cell from its bulk ampoule using a blown air heat gun. The bulk rubidium stays out of the cell to keep it from interacting with the paraffin. The cell is then separated from the glass apparatus by melting the glass pipe just above the rubidium [23]. Figure 2.8 shows a conventional atomic vapor cell.

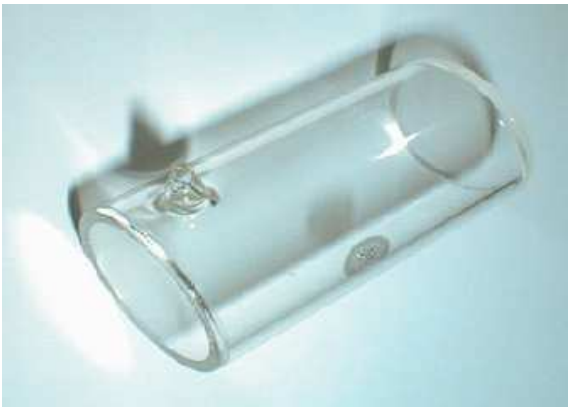

Figure 2. 8 A conventional atomic vapor cell.

2.6 Vapor Cell Integration Advantages

Integrating the vapor cell into a hollow waveguide increases the interaction length of light with vapor and decreases the mode size of the interacting beam; both effects significantly enhance the nonlinear effects. A spot size comparable to the absorption

cross section of the atom, $3\lambda^2/2\pi$, is necessary for low level quantum interference effects [24] and to enhance nonlinear effects [11]. For the D_2 transition in rubidium the absorption cross section is approximately 3 μm^2, which corresponds to a .6 μm spot size. A beam with a 4 μm waist provides a close match and gives a 31 μm focal depth [11]. A longer interaction length would also enhance the nonlinear effects. However, increasing the focal depth of the beam increases the beam waist, making it much larger than the absorption cross section. Thus, the focal depth and the spot size of beams are coupled and the interaction with vapor in a conventional cell is limited. Integrating the cell into a hollow waveguide allows for long interaction lengths as well as small mode confinement. As long as the light is confined within the absorption cross section-sized core the light will interact with the alkali vapor and significantly enhance the nonlinear effects throughout its length. For example, integrating the alkali vapor into a hollow waveguide 7 mm long would increase the nonlinear interaction length 225 times over a conventional cell. Not only would the nonlinear interaction length increase, the overall size would decrease, thus making it more viable for commercial use.

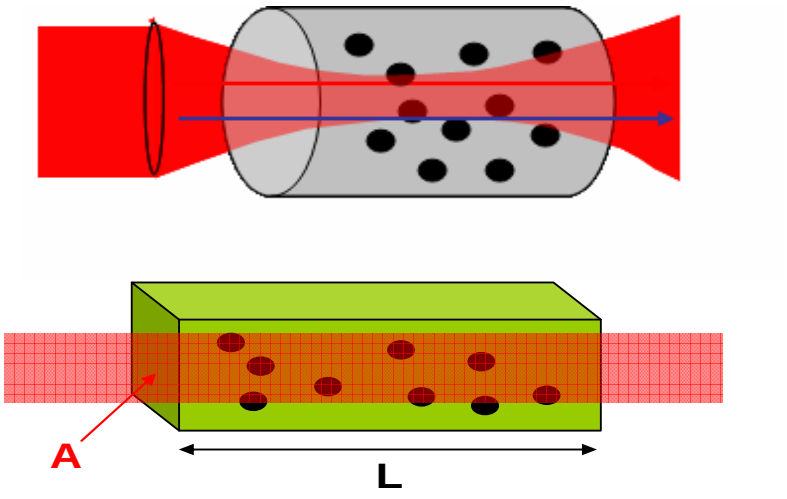

Figure 2. 9 A hollow waveguide allows for small mode confinement and long interaction lengths. Conventional cells do not allow for both.

2.6.1 NIST Reference Cell

The National Institute of Standards and Technology (NIST) recently developed its own miniaturized vapor cell. The cell was created mainly for use as a miniaturized atomic clock [10], although it also has potential uses as a magnetometer, an apparatus for spectroscopy, and as a frequency reference cell. The cell could not be fabricated using traditional glass blowing techniques, because of the desired small scale [10]. To fabricate the cell on the millimeter scale, silicon micromachining was used. This actually lowered the cost and created a device that was more highly reproducible than any glass blown device [10]. The atomic frequency reference came from either rubidium [25] or cesium [10, 26] atoms in the cell. Both of these atoms react with many materials and cannot be handled in the air. Therefore a special fabrication method was developed to avoid specimen contamination.

The devices are fabricated using micromachined silicon and borosilicate glass anodically bonded together. To begin the fabrication process double-sided polished <100> wafers were photolithographically patterned and etched. Then, using high temperature and a high electric field, a similarly sized piece of borosilicate glass was anodically bonded to the silicon. This caused oxide to form at the interface and create a hermetic seal [10]. At this stage a small cavity has been formed, which the alkali atoms can be placed into. Figure 2.10 shows the steps to fabricating an NIST cell.

The alkali atoms were introduced into the cavity in two ways. The first method involved using chemical reactions of BaN_6 in H_2O and Alkali-Cl to form an elemental alkali atom in an ultra high vacuum environment [10]. The ultra high vacuum environment allows for fairly precise control of the pressure and the gases in the

environment. After the elemental alkali atoms have been formed the chamber can be backfilled with a buffer gas to an appropriate pressure. In this environment the top borosilicate glass piece is anodically bonded onto the cell cavity.

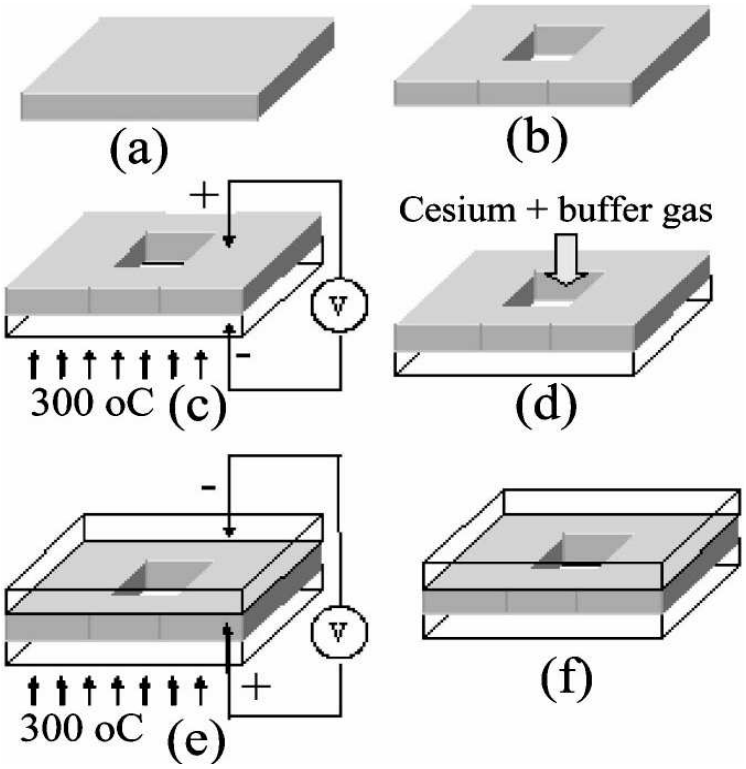

Figure 2. 10 The fabrication process for the NIST reference cell [10].

The second method for incorporating alkali atoms into the cell cavity utilizes an anaerobic glovebox filled with dry nitrogen [10]. This method works well for cesium which is liquid at room temperature. A nanoliter pipette transfers the liquid cesium directly from an ampoule to the cell cavity. The cavity is then placed in a low vacuum bell jar, in which the buffer gas is added and the top borosilicate glass is anodically

bonded to the cell cavity. Figure 2.11 shows cesium absorption spectroscopy peaks from the cell. Although, the NIST cell does miniaturize the conventional atomic vapor cell, it does not improve the interaction length of the beam with the atoms.

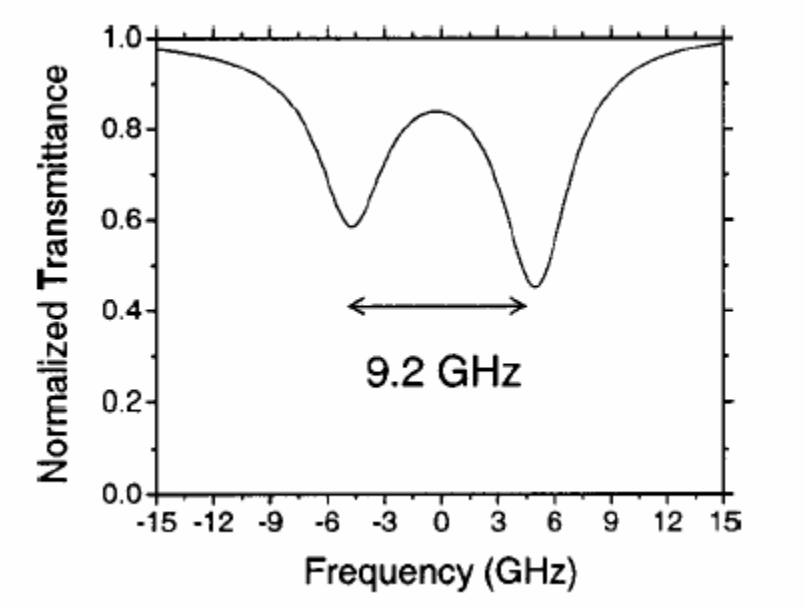

Figure 2. 11 Absorption spectrum of cesium in the NIST reference cell, frequency units show the difference in frequency between dips [10].

2.6.2 Photonic Band-gap Fiber

Photonic band-gap fibers (Figure 2.12) have been integrated with rubidium and other atomic vapors for saturated absorption spectroscopy (Figure 2.13) [27] and to exhibit other optical effects [28]. Photonic band-gap fibers confine high intensities of light in a hollow region using photonic structures which surround a hollow core. To incorporate rubidium vapor into the photonic band-gap fiber the fiber must first be prepared with monolayer coatings [24]. Like paraffin in conventional cells, these coatings limit the number of atoms which adsorb onto the silica walls of the fiber. After the

coating, the ends of the fiber are placed in separate vacuum cells. One cell contains rubidium, which diffuses down the length of the fiber [24]. The optical measurements take place while the fiber is hooked up to the vacuum cells. However, the fibers must be sealed in the optical path and the non-planar setup of the fiber limits the optical interaction to a single dimension.

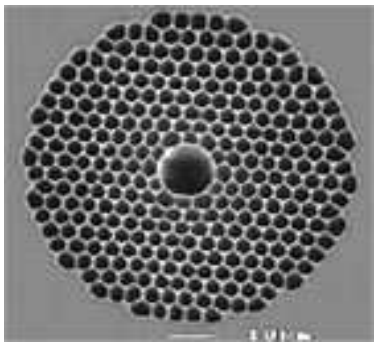

Figure 2. 12 SEM of a photonic band-gap fiber.

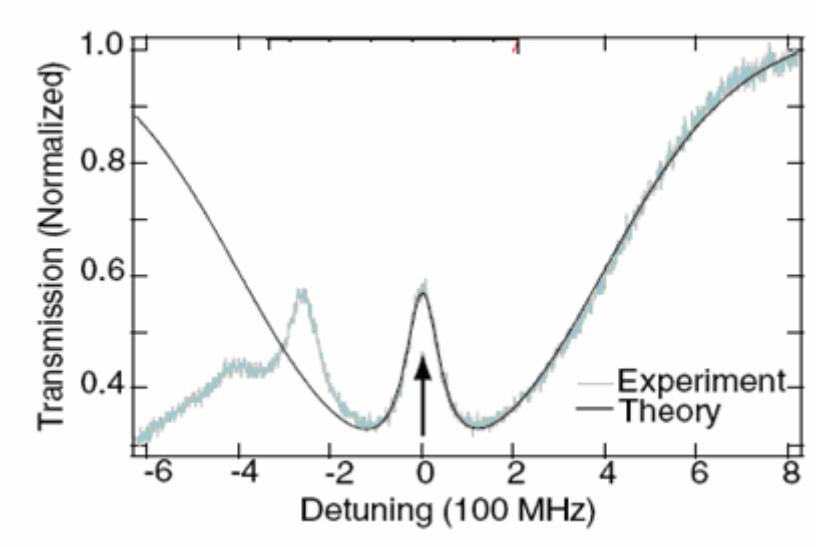

Figure 2. 13 Saturation absorption spectrum in photonic band-gap fiber [27].

3 ARROWs

3.1 Principle

Unlike conventional waveguides, ARROWs do not guide light through total internal reflection at a single boundary [29]. Conventional optical waveguide designs require that light propagates in a high index medium surrounded by a lower index one, this allows total internal reflection. If the core had a lower index of refraction, light would quickly leak into the surrounding higher index material. ARROWs allow light to propagate in lower index media by utilizing Fabry-Perot reflectors in the transverse direction. The Fabry-Perot reflectors act like mirrors, exhibiting high reflectivity when operating at anti-resonance [29]. The finite transmission of the cladding layers makes the ARROW a leaky waveguide. However, the loss reduces when more dielectric layers are added. Each additional layer decreases the loss by approximately three times [30]. The ARROW is also effectively a single mode waveguide since higher order modes are suppressed by high optical losses [29]. To achieve the anti-resonant, highly reflective condition the dielectric layers must be deposited to a fairly precise thickness determined by Equation 2 [29]:

$$t_j = \frac{\lambda}{4n_j}(2M+1)\left[1-\frac{n_c^2}{n_j^2}+\frac{\lambda^2}{4n_j^2 d_c^2}\right]^{-1/2}. \qquad (2)$$

In the equation n_j and n_c are the index of refraction of the jth layer and the core, respectively, d_c is the thickness of the core, λ is the wavelength, and M is an integer representing the anti-resonance order. These correspond with Figure 3.1, which shows a cross section of an ARROW.

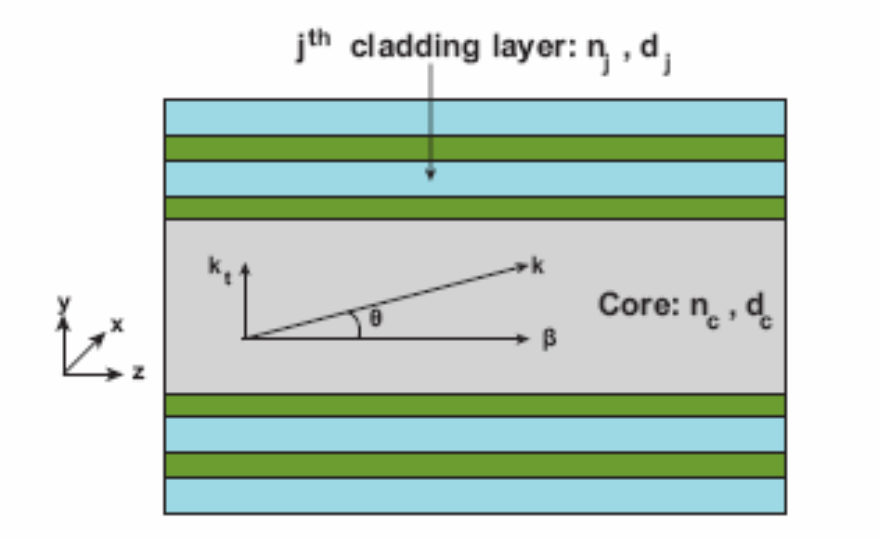

Figure 3. 1 Cross section illustration of an ARROW waveguide.

3.2 Fabrication

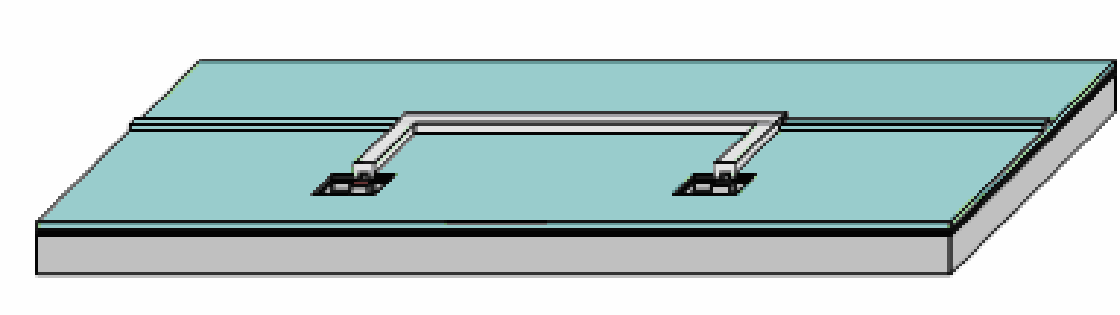

Figure 3. 2 ARROW platform.

The ARROW fabrication process utilizes standard semiconductor processes [30, 31]. This makes fabrication of multiple devices simultaneously possible. ARROWs are fabricated on <100> crystal orientation silicon wafers to allow the devices to be cleaved perpendicular to the waveguides. The process for fabricating the device shown in Figure 3.2 begins by depositing the bottom dielectric layers of silicon dioxide and silicon nitride using plasma enhanced chemical vapor deposition (PECVD). Each layer thickness is deposited according to Equation 2. Following the bottom layers the sacrificial core is fabricated using SU-8 spun on to a specified thickness, patterned, and developed (Figure 3.3). The top dielectric layers are then deposited over and around the sacrificial core using PECVD (Figure 3.4). The top oxide layer is deposited thicker than the other layers, but still at an anti-resonant thickness. This thick oxide layer provides structural strength for the waveguide [32]. Ridge waveguides etched into the top, thick silicon dioxide layer provide a means for coupling light into the hollow core without exposing the hollow waveguide to the surrounding air [33], which is essential to atomic vapor cell success. The solid-core, ridge waveguide is patterned with an SU-8 mask and etched using a reactive ion etcher (Figure 3.5). The next step is to expose the sacrificial cores to air to allow them to be etched and removed. This is also done in the reactive ion etcher with the pattern masked by SU-8 (Figure 3.6). To complete the ARROW and make it hollow, a highly selective acid bath etches the sacrificial core (Figure 3.7). The openings in Figure 3.7 can now be used to attach a reservoir that does not interfere with the optical beam path. Figure 3.8 shows a cross section of a completed ARROW.

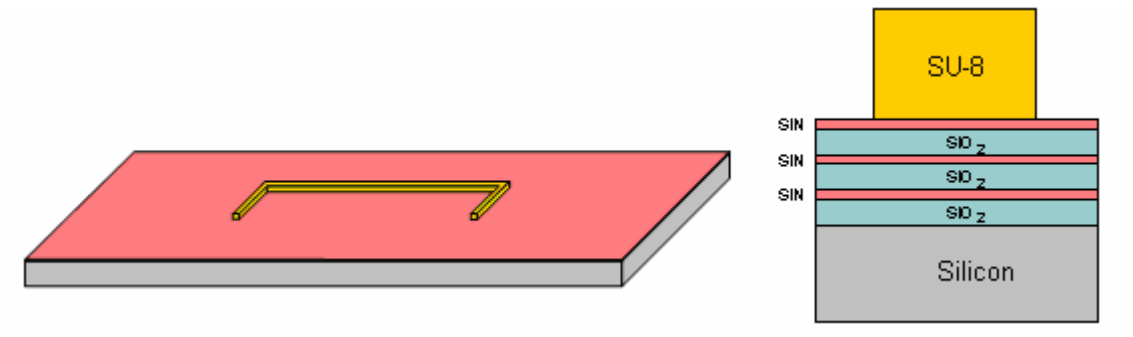

Figure 3. 3 Bottom dielectric layers and sacrificial core deposited.

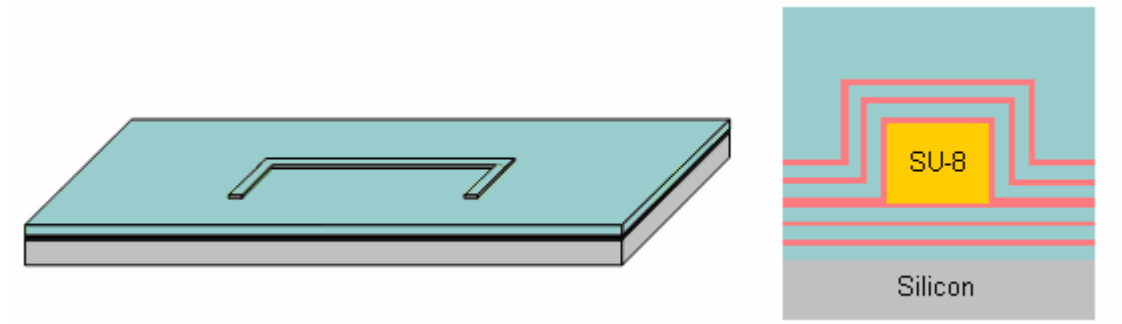

Figure 3. 4 Top dielectric layers deposited over core, with a thick top oxide layer.

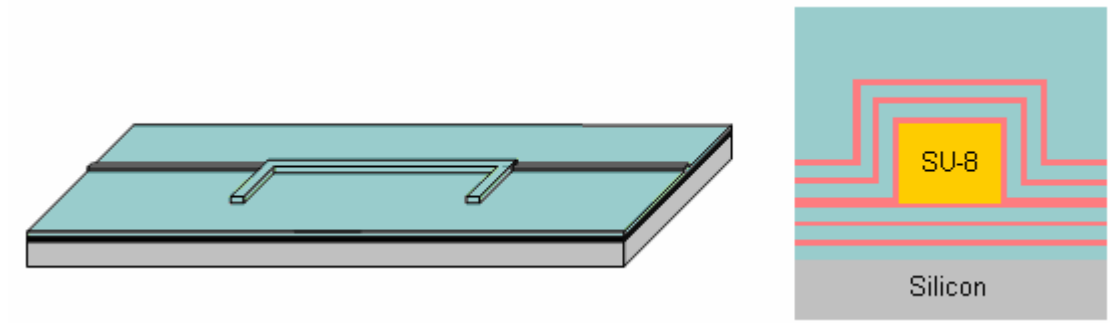

Figure 3. 5 Solid-core waveguides etched into the thick, top oxide layer.

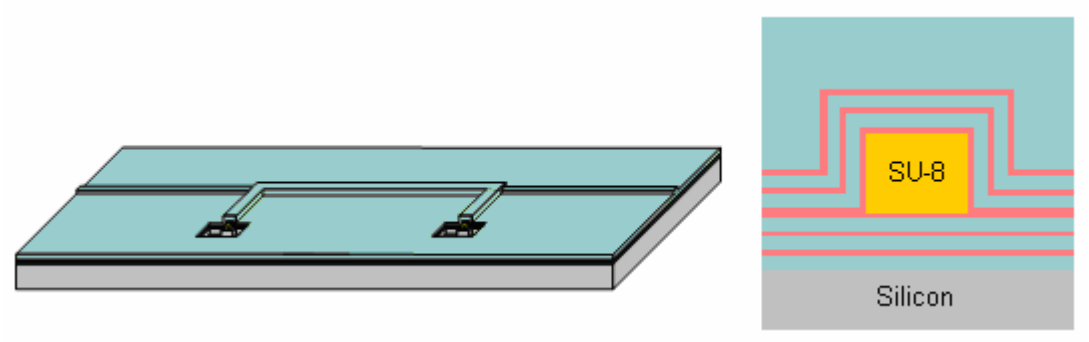

Figure 3. 6 Sacrificial cores exposed through etching.

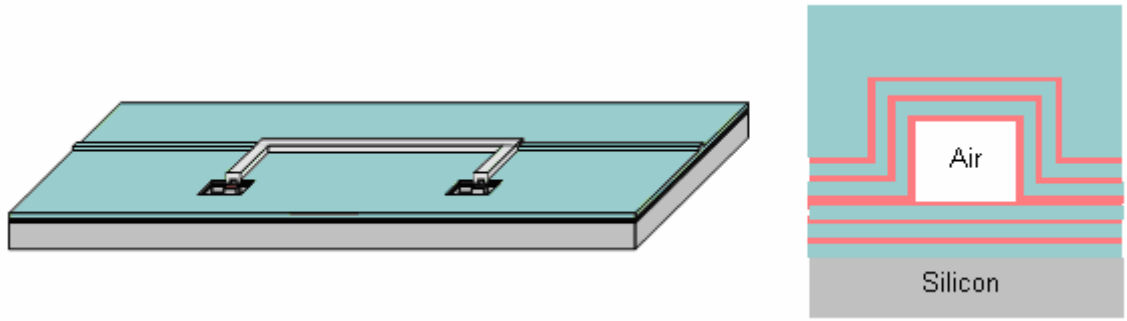

Figure 3. 7 sacrificial cores etched out in selective acid etch.

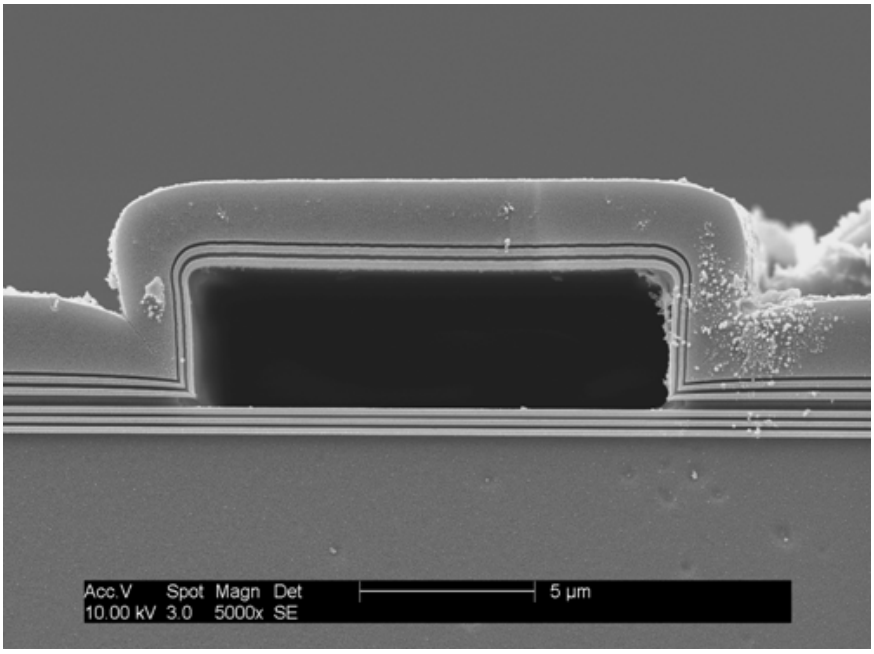

Figure 3. 8 SEM cross section of an ARROW looking into the hollow core.

3.3 Variations in Design

Several different geometries can be fabricated to give hollow waveguides unique characteristics. The fabrication process outlined above (Section 3.2) yields a rectangular core (Figure 3.8) [30, 34]. The thick top oxide layer extends laterally out from the waveguide as can be seen in the figure. This high index layer yields a higher loss in the waveguide than if air were laterally extending out from the waveguide. Fabricating the ARROW on a raised pedestal creates a waveguide where air extends laterally from the waveguide [30, 34]. This is realized by adding a single step to the fabrication process. Before depositing the bottom dielectric layers the pedestal is etched into the silicon. This places the lateral extensions of the waveguide above the thick top oxide layer [30, 34]. Figure 3.9 shows a cross section of a pedestal ARROW.

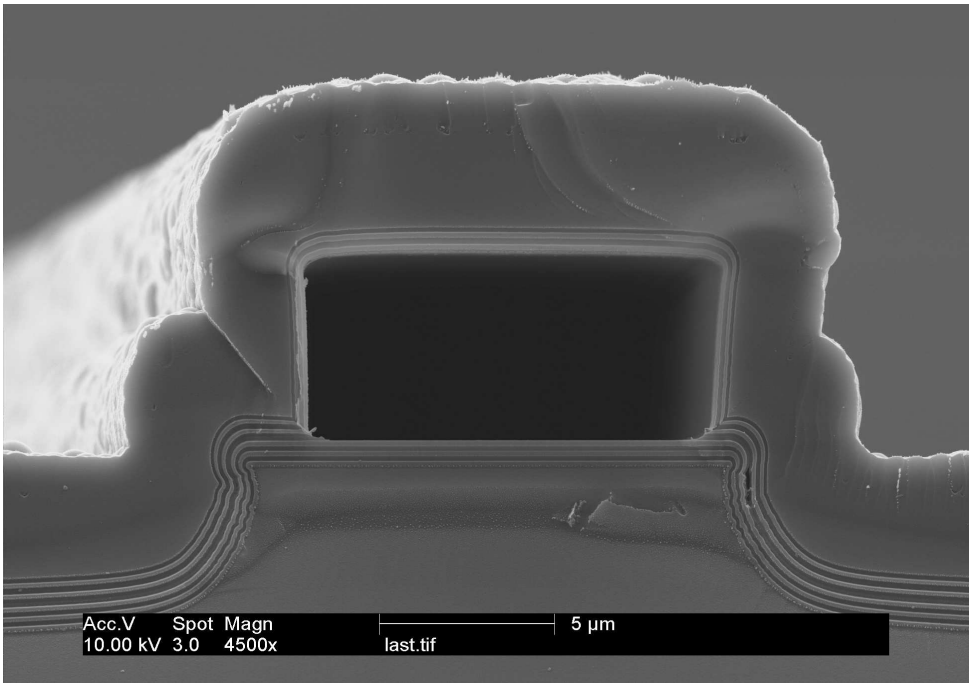

Figure 3. 9 SEM cross section of a pedestal ARROW

The shape of the core can also be changed to give different waveguiding properties. Fabrication processes have been developed to make an arched core ARROW (Figure 3.10) [35]. The arched core ARROW improves the structural strength of devices, provides lower loss, and is less polarization dependent than rectangular cores [36].

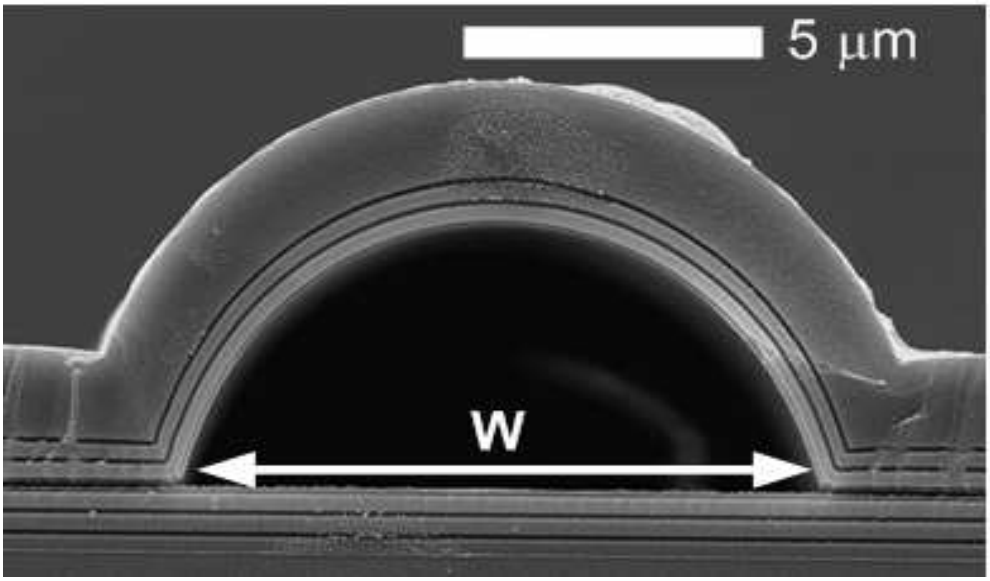

Figure 3. 10 SEM cross section of an arched-core ARROW.

3.4 ARROWs for Vapor Cell Integration

ARROWs provide attractive platforms for atomic vapor cell integration. Like photonic band-gap fibers, ARROWs decouple the tradeoff between small beam area and finite focal depth. The ARROW provides long interaction distances, with a high optical density of atoms, which provides large intensities over these distances. Also, the hollow waveguide aligns any beams propagating through its core, taking away the hassle of aligning multiple beams in an atomic vapor cell. However, unlike photonic band-gap

fibers ARROWs are a fully planar, monolithically integrated device, which utilizes standard semiconductor fabrication techniques. Monolithic integration of the ARROW provides intersecting solid core waveguides with the hollow core ARROW. This waveguide intersection provides a means for resonant fluorescence detection, simplified Doppler-free spectroscopy, and parametric generation. Also, the interface between the hollow core ARROW and the solid core waveguides is essential for sealing the hollow core and allowing beams from off chip to interact with atoms in the sealed, hollow core (Figure 3.11). Also, with a footprint of about 1 cm^2, the ARROW device is smaller than both the NIST cell and photonic band-gap fibers. The ARROW also provides significant improvement to the overall volume, optical volume, and intensity of the interacting, propagating beam. Table 3.1 provides a comparison between the volumes and intensities of the bulk atomic vapor cell, the NIST cell, and the ARROW. As the table shows the ARROW provides several orders magnitude of improvement over the bulk and NIST cells volume and overall volume.

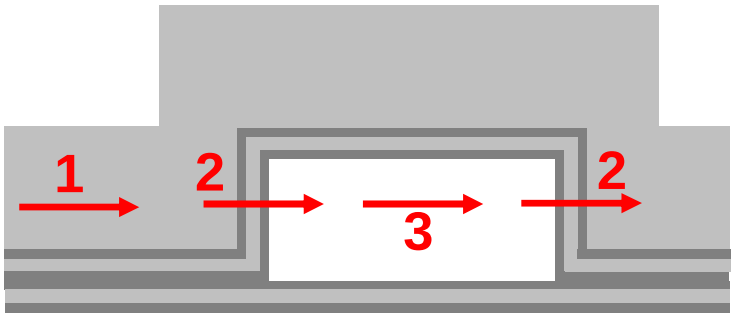

Figure 3. 11 The interface (2) between the solid core (1) and the hollow core waveguides (3) allows the integrated vapor cell to be sealed.

Table 3. 1 A comparison of the overall volume, optical volume, and intensity in bulk cells, NIST cells and the ARROW.

	dimensions [um x um x um]	**V [pl]**	**Vopt [pl]**	**I [norm.u.]**
Bulk cell	25,000 x 25,000 x 50,000	3.1×10^{10}	4×10^{7}	1
NIST cell	1000 x 1000 x 1000	1,000,000	23,000	35
ARROW	5 x 12 x 7000	420	200	62,000
ARROW Improvement	**Mode area: 19 l2**	7.4×10^{7} (bulk) 2,400 (NIST)	3×10^{5} (bulk) 115 (NIST)	62,000 (bulk) 1,700 (NIST)

4 Vapor Cell Integration with ARROW

4.1 ARROW Vapor Cell Platform

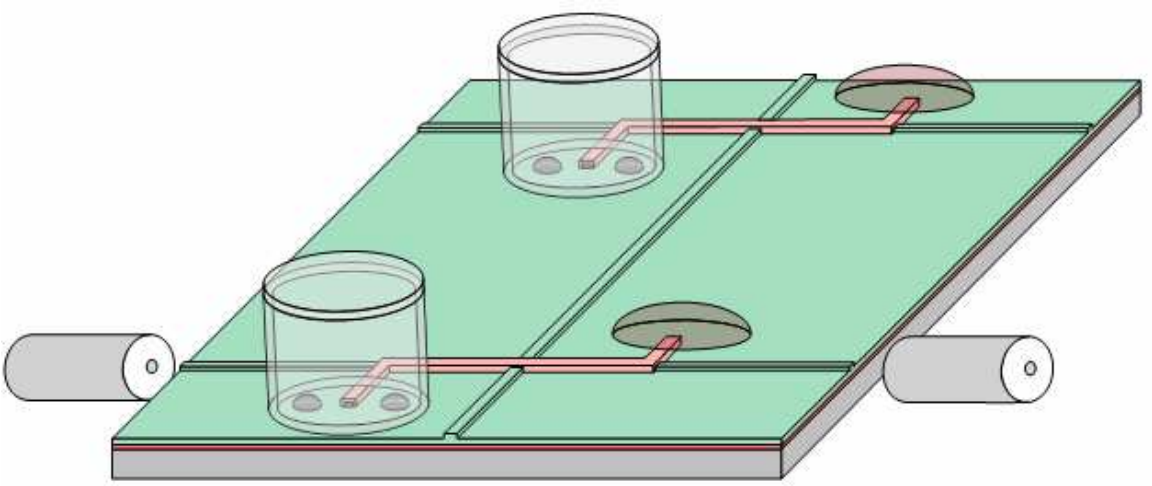

Figure 4. 1 The integrated vapor cell platform using ARROWs.

The ARROW platform was designed to be integrated with vapor cells. Figure 4.1 shows many of the features used in the design of the integrated platform. The hollow core waveguides are designed in an S-shaped pattern. This design allows vapor cell integration without covering the light-guiding segment of the hollow waveguide. Also, the sealed end of the hollow core waveguide can be sealed away from the light-guiding segment of the waveguide. Ridge waveguides etched into the thick, top oxide layer allow light to be coupled into the hollow core waveguide without exposing the hollow cores to air (Figure 3.11). All coupling of light onto the chip is done with the ridge waveguides. Ridge

waveguides can also be used for intersections which would be useful for applications like resonance fluorescence detection, parametric generation, and Doppler-free spectroscopy [37]. Also, multiple devices can be put on the same chip, as Figure 4.1 shows.

4.2 Vapor Cell Attachment

The integration of vapor cells with the hollow waveguide presents unique challenges. The most common method for transferring vapor into a vapor cell is to move a solid source of alkali atoms to the inside of the vapor cell. Once the alkali atoms are in the vapor cell, it must provide a stable, hermetically sealed, and inert environment. Any oxygen initially in the cell or leaking in will contaminate the vapor or the bulk sample. The seal must be stable for long periods of time to ensure that the device is usable for that time. To seal the vapor cell to the substrate the vapor cell must seal onto the flat substrate as well as over the waveguides which rise to at least ten microns above the substrate. This generally means that some type of epoxy, which can flow around the waveguide and seal, is required to seal the vapor cell over the waveguide. Also, some way of adjusting the pressure within the cell would be desirable for quantum interference effects. This would reduce the number of collisions between rubidium and buffer gas atoms and lower the coherence dephasing rate of the alkali atom.

4.3 Leak Rates for the Vapor Cells

Using the device specifications described in Section 4.2 several sealing techniques were tested for compatibility with the integrated cell platform. Here a representative

sampling of the techniques is presented. The techniques and materials presented were tested for their unique characteristics. Sealing adhesives tested include silicone and five-minute epoxy. Rubber stopper sleeves, which fit tightly around glass tubes, were also tested to determine how well natural rubber would seal. Butyl rubber o-rings sealed tightly with screws were tested, as were Swagelok fittings, which showed how well a metal-metal connection would seal.

The vapor cell seals were tested by measuring the leak rate of helium gas out of the cell. The devices were fabricated and sealed in a helium filled glovebox which left helium gas inside each vapor cell. The vapor cells were then tested in a helium leak detector. The leak rate of helium gas out of the cell determined how well the sealing mechanism worked.

The vapor cells used to test the sealants, silicone and epoxy, were fabricated in the same way. A 4 mm outer diameter and 2 mm inner diameter glass tube cut to 1 cm in length was used as the vapor cell. To seal the glass tube, two 1 cm square glass pieces were attached to both sides of the cut glass tube using either silicone or five minute epoxy. This process took place in a helium atmosphere glovebox, thus leaving helium gas inside the cell. The helium leak detector measured a leak rate of 3.225×10^{-7} mbarL/s for the silicone cells and 0.134×10^{-7} mbarL/s for the epoxy. The silicone leak rate proved to be the worst leak rate out of all the designs.

The rubber stopper sleeve vapor cell leak rate offers some improvement in leak rate over the silicone. The rubber stopper sleeve works by fitting snugly over the end of a 4 mm outer diameter glass tube. The end of the glass tube not sealed with the rubber stopper sleeve was sealed with a 1 cm square glass piece epoxied to the glass tube. The

epoxy use was justified by its low leak rate. Many types of adhesives were used to seal the stopper sleeve to the glass tube. However, these proved to be no better than just fitting the stopper sleeve over the glass tube, showing that the rubber stopper sleeve had a higher leak rate than the sealants. The helium leak detector measured leak rates of 1.991×10^{-7} mbarL/s for this vapor cell.

The screws with o-ring and Swagelok cells both had low leak rates. Tapped holes drilled into bulk aluminum, but not all the way through, served as the cell for the screw and o-ring vapor cells. This allowed the cells to be isolated with no paths for helium leakage, other than through the o-ring. In the glovebox, a screw with a butyl o-ring was screwed into the tapped hole. The o-ring provided a good seal for the helium remaining inside the cell. This method yielded leak rates similar to those of the epoxy: 0.137×10^{-7} mbarL/s. To test the metal-metal sealed vapor cell, both sides of small Swagelok fittings were sealed in the glovebox. No leaks were detected with these seals.

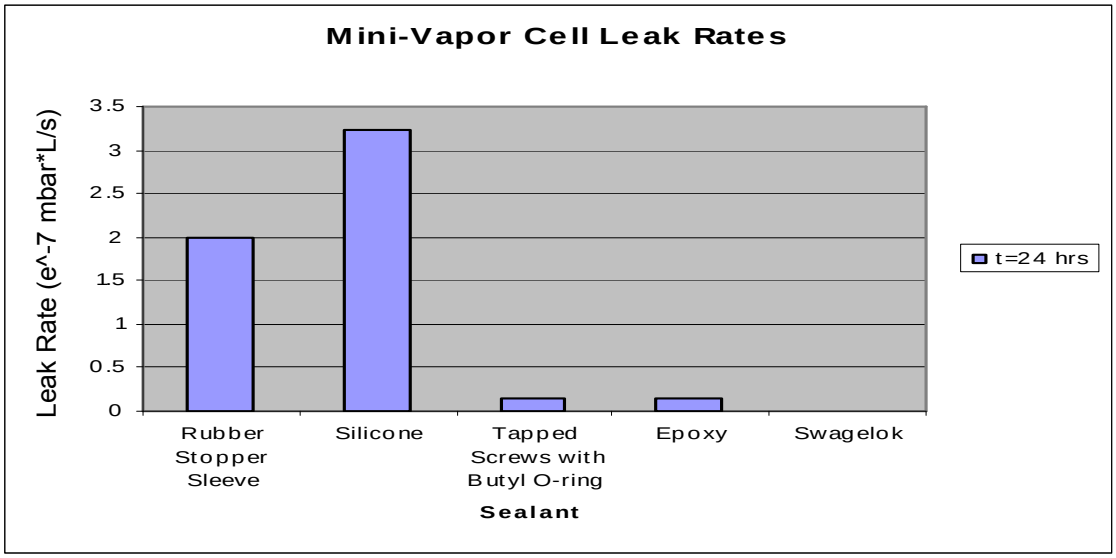

Figure 4. 2 Leak rates of various sealing techniques tested for possible integration with hollow waveguide.

These tests revealed that the epoxy, o-ring/screw, and Swagelok cell fabrication methods would provide the best seal. However, the sensitivity of the alkali atoms to the vapor cell required further testing. To do this vapor cells were created and the rubidium was monitored. Rubidium's contamination was apparent as its color within the cell would change from silvery to white, green, or violet. These tests revealed that epoxy could only be used as a sealant as long as it had cured before the alkali atoms were introduced to the cell: the outgassing of the epoxy as it cured contaminated the alkali sample. Also, certain metals used for the o-ring and screw technique would contaminate the sample: aluminum turned the rubidium white and brass turned it green. Stainless steel proved to be the most compatible with the alkali atom sample. The cells used for the measurements discussed in the following sections were fabricated using the epoxy as well as the o-ring/screw fabrication techniques.

4.4 Rubidium Incorporation into Vapor Cell

Rubidium incorporated into the vapor cell serves as the alkali vapor in this apparatus. Despite rubidium's benefits for quantum interference it has many characteristics which make it difficult to use. Rubidium is known to ignite in air, react violently in water, and react with many other materials. Even moisture in the air contaminates rubidium and slight amounts of oxygen oxidize it. For this reason all transferring of rubidium is done within the inert atmosphere of a glovebox.

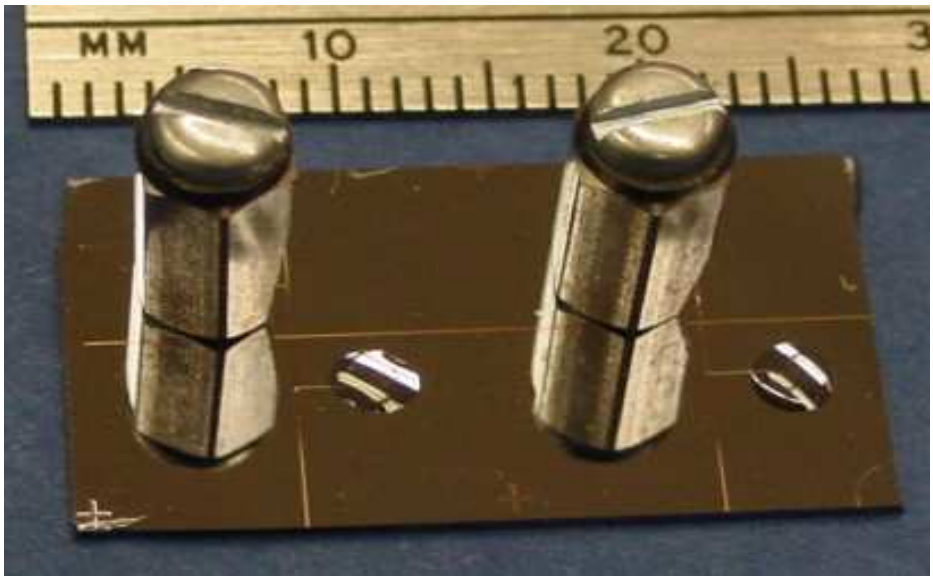

Figure 4. 3 Photograph of the integrated vapor cell platform with an ARROW.

Rubidium integration onto the hollow waveguide platform utilizes the stainless steel and epoxy vapor cell discussed at the end of Section 4.3 (Figure 4.3). The stainless steel vapor cell is modified to fit on the platform. The modification involves thinning one of the side walls so the vapor cell does not overlap the ARROW waveguide on the chip. After cleaning and dehydration baking the stainless steel standoff, it is epoxied to the ARROW chip over an open end of the hollow channel (Figure 4.4b). A dab of epoxy over the channel's remaining open end is necessary for the cell to be sealed. Passing the waveguide into the glovebox's inert atmosphere prepares the device for rubidium incorporation. Once the bulk rubidium in an ampoule liquefies at 39 C, stainless steel implements transfer small amounts to the inside of the stainless steel vapor cell. Sealing the vapor cell occurs once a stainless screw is screwed into the standoff. An o-ring placed on the screw seals the vapor cell and the hollow channel (Figure 4.4c). This completely fabricated vapor cell can now be tested for atomic spectroscopy.

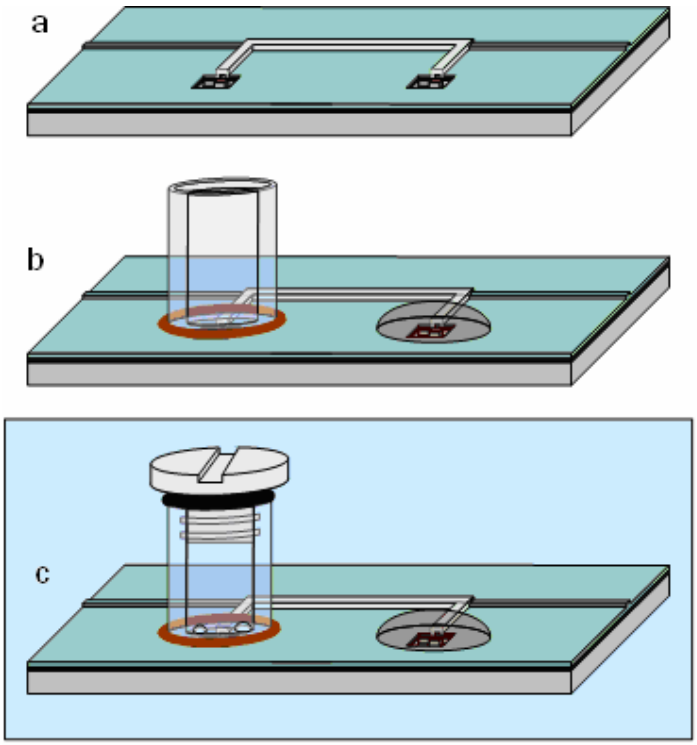

Figure 4. 4 Diagram showing process used to incorporate rubidium into the vapor cell, a) fabricated hollow channel, b) vapor cell is integrated onto the waveguide chip, and c) in an inert atmosphere rubidium is incorporated into the cell.

4.5 Self Assembling Monolayer Coating

Of particular concern for rubidium filled cells is adsorption of rubidium to the silica glass walls [29]. Rubidium within cells will adhere to the walls and lose their effectiveness in interacting with the light. Also, spin-decoherence, which occurs as rubidium atoms interact with the walls, makes creating quantum interference effects difficult. The adsorption of the rubidium has been addressed in large rubidium cells by coating cell walls with paraffin or siloxane monolayers [29, 38]. These passivate the

surface of the silica glass. This decreases both the occurrence of rubidium atoms adhering to the wall and the number of rubidium atom interactions with the cell wall, thus increasing the effectiveness of the vapor cell as a quantum interference device. Similar adsorption problems occur with the silicon nitride wall surface in the ARROW devices. Fortunately, the same methods which improved the problem can do the same for the silicon nitride walls. A paraffin layer, the passivation coating layer on conventional cells, does not provide an attractive passivation coating. Paraffin coatings are typically done through evaporation in a vacuum. The small, confined dimensions of the ARROWs make it difficult to evaporate paraffin inside the channel. However, siloxane monolayers, such as octadecyldimethylmethoxysilane (ODMS) can be formed in the liquid state (Figure 4.5) [39]. For this reason siloxane monolayers are the preferred method for passivation of ARROW walls.

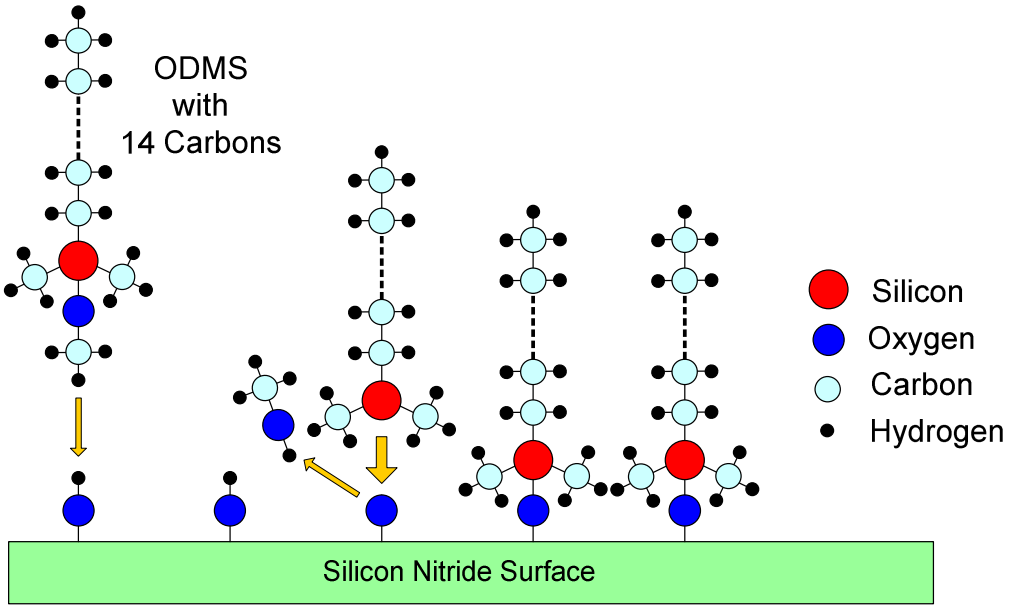

Figure 4. 5 ODMS Self assembled monolayer on the silicon nitride surface.

The effectiveness of self-assembled monolayers is well documented; however it's effectiveness on PECVD silicon nitride surfaces is not. Dyne pen tests were used to find the effectiveness of these coatings on the PECVD silicon nitride surface. Dyne pens come in several different dyne level fluids. The surface energy of the surface can be found by applying a thin layer of dyne pen solutions to the surface and noting the time taken for the solution to bead. If, for example, a 50 dyne pen is applied to the surface and it beads within two seconds, the surface energy is 50 dynes/cm. If the 50 dyne fluid takes longer than two seconds to bead, higher dyne level pens should be used until the fluid beads within two seconds. Using this technique for uncoated PECVD silicon nitride yielded a surface energy of 60 dynes/cm. Dyne tests were then conducted on ODMS, HMDS, paraffin, Surpass 4000, and Ultratol Dynamic coated samples. The results can be seen in Table 4.1. Tests showed the surface energy can be reduced using ODMS, HMDS, or paraffin. ODMS is the preferred method of surface passivation, because of the difficulty of depositing paraffin and the limited adherence time of HMDS.

Table 4. 1 Effectiveness of passivation layers in lowering the surface energy of PECVD silicon nitride.

	Uncoated	**ODMS**	**HMDS**	**Paraffin**	**Surpass 4000**	**Ultratol Dynamic**
PECVD Nitride surface energy	60 dynes/cm	50 dynes/cm	40 dynes/cm	40 dynes/cm	>60 dynes/cm	>60 dynes/cm

A method for coating the walls of the hollow channel waveguide is still being developed. Currently, straight hollow channels can be coated with little affect on its waveguiding properties. However, coating the S-shaped channels used for the integrated vapor cell platform ruins the waveguiding. The self-assembled monolayers will coat the corners too thickly and block the transmission path of the laser.

5 Optical Measurements

5.1 Vapor Cell

Before integrating the vapor cells with the hollow waveguides, the vapor cells effectiveness was tested. Several effects could ruin the vapor cell by contaminating the rubidium: leaks in the cell, outgassing of any adhesives used in the fabrication, dirty glass, or reaction with the metal. Any of these would destroy the rubidium absorption spectrum. Tests to measure the rubidium absorption spectrum in these vapor cells proved the effectiveness of the vapor cell.

Several techniques were employed for making the vapor cells for testing. The results presented here used 4 mm outer diameter and 2 mm inner diameter glass tubes cut down to 1 cm lengths. The ends of these cut tubes were flattened, polished, cleaned, and then attached to a glass substrate using epoxy. Rubidium droplets were transferred to the cell in the inert atmosphere of a glovebox as discussed in Section 3.4. Placing a rubber stopper sleeve over the glass tube completed the fabrication. A laser probed through the glass reservoir to test for the rubidium absorption spectrum. The absorption platform was set up as seen in Figure 4.1. Figure 4.2 shows the absorption spectrum through this cell (bottom curve) compared to a bulk rubidium cell (top curve). The less pronounced absorption peaks are a result of the smaller size of these vapor cells compared to the bulk cell.

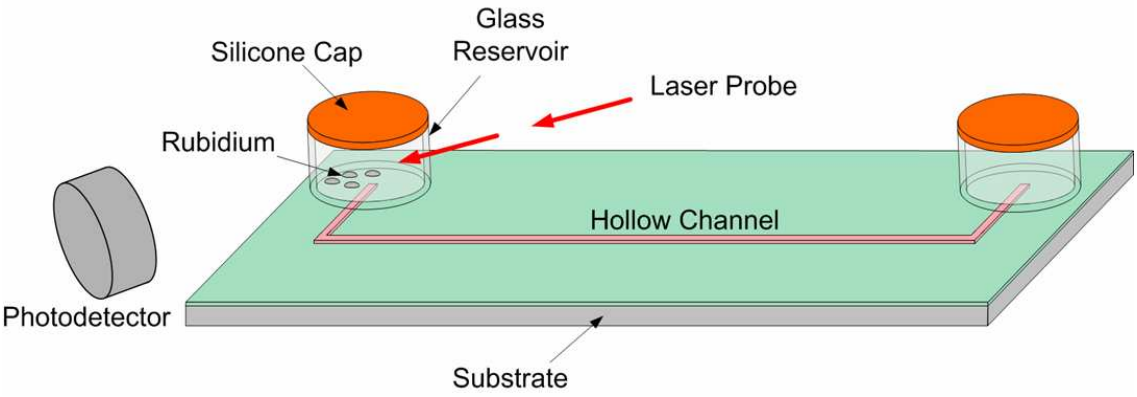

Figure 5. 1 Test platform for the rubidium filled vapor cell absorption test.

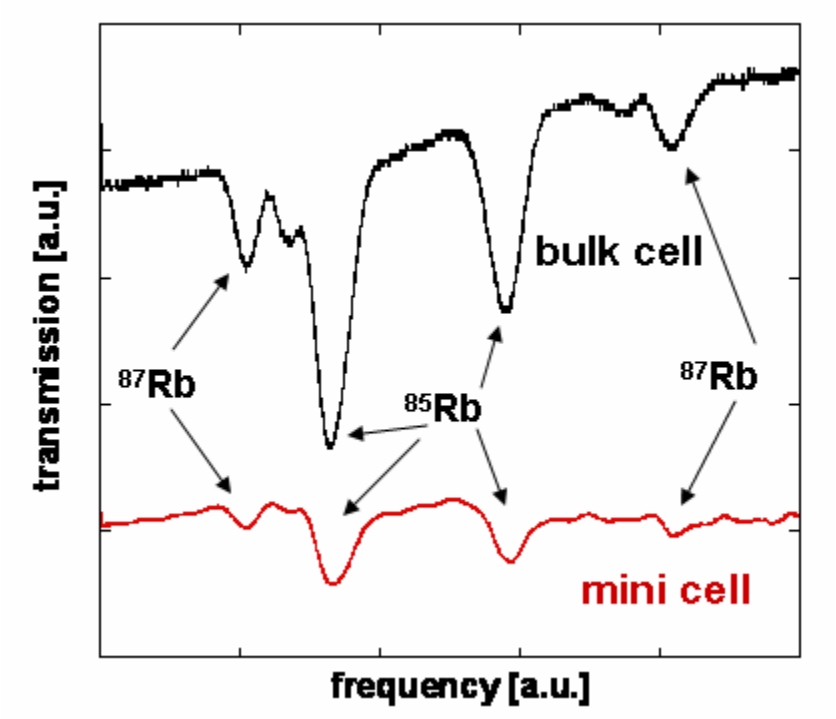

Figure 5. 2 Measured absorption spectrum from the rubidium filled vapor cell around the D_2 line.

5.2 Vapor Through Channel

After obtaining a rubidium absorption spectrum in a vapor cell a test was developed to verify whether rubidium vapor would travel through an ARROW-sized channel to another vapor cell. This platform utilized a hollow channel fabricated using techniques similar to those discussed in Section 2.2, except that the channel did not have alternating dielectric layers. Cut glass tube vapor cells were placed on the platform using epoxy, just as in the experiment above. Likewise, the rubidium was placed in the vapor cell using the same technique. However, rubidium was placed in only one cell.

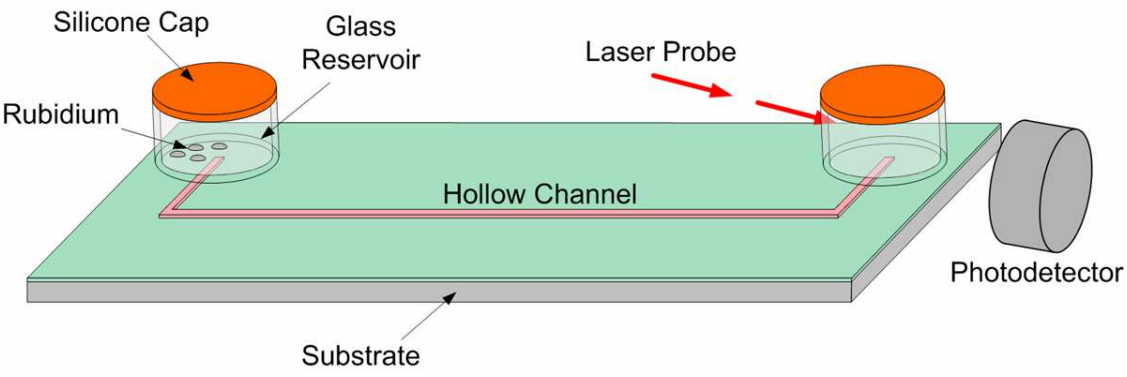

Figure 5. 3 Test platform for measuring rubidium absorption in empty vapor cell connected to rubidium filled vapor cell through hollow channel.

For the experiment a laser was probed through the vapor cell that rubidium was not placed in. Figure 4.3 shows the experiment platform. Absorption was detected on the output of the vapor cell as seen in Figure 4.4. This showed the rubidium vapor traveled through the small dimensions of the hollow channel.

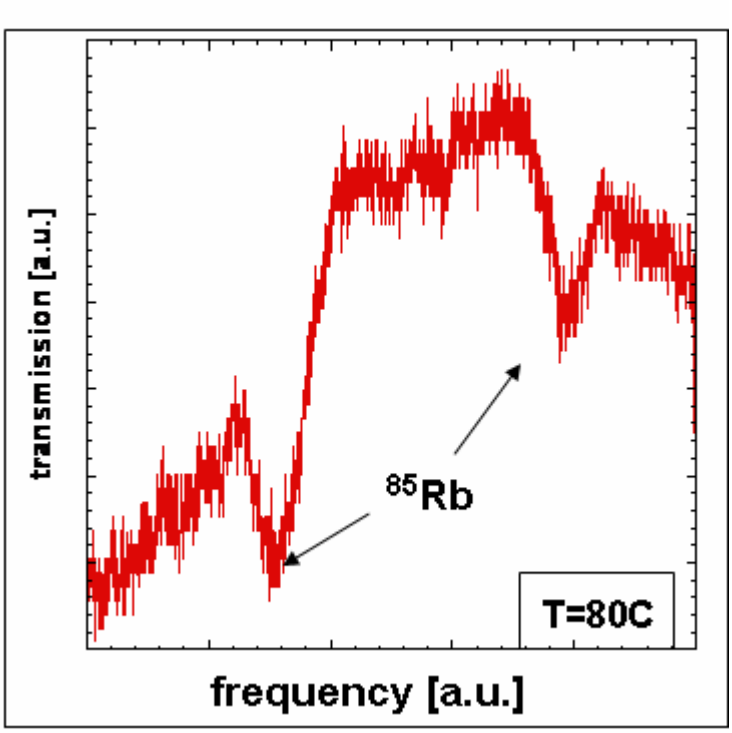

Figure 5. 4 Measured absorption peaks in the empty vapor cell connected to rubidium filled vapor cell through hollow channel.

5.3 Absorption Spectroscopy in ARROW

The next experiment probed through the ARROW channel integrated with rubidium atoms to look for absorption dips. The devices used for testing were fabricated using the ARROW fabrication techniques discussed in Section 2.2. After the ARROW devices were ready a vapor cell was epoxied to an open end of the ARROW as discussed in Section 3.4. The devices were tested by coupling the laser into the solid core waveguide. After passing through the solid core the laser light passed through the solid to hollow core interface. Once in the hollow core waveguide the light interacted with the rubidium atoms. The light propagated out of the hollow core and back into a solid core waveguide. A detector placed on the opposite end of the device detected the light coming

out. Figure 4.5 shows the experiment platform used. Figure 4.6 shows the absorption spectrum of the rubidium D_2 line around 780 nm. Both the ^{85}Rb and ^{87}Rb absorption peaks are visible.

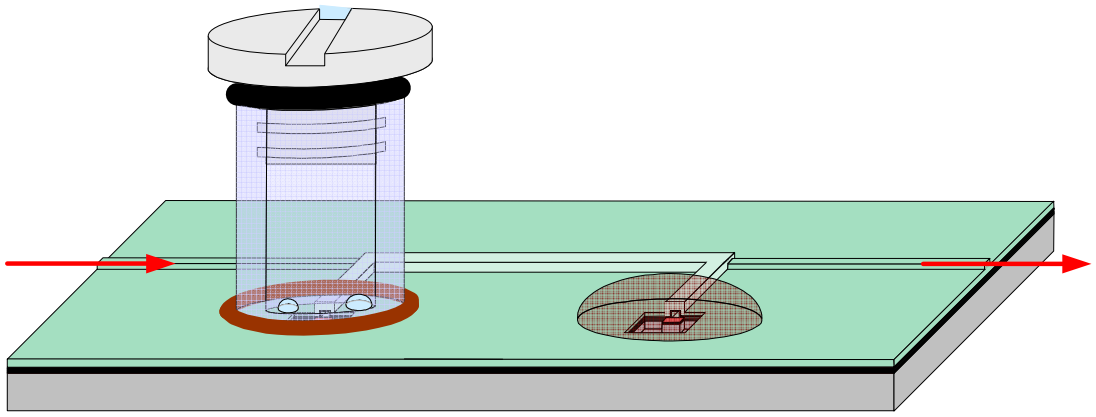

Figure 5. 5 Absorption spectroscopy setup using the ARROW.

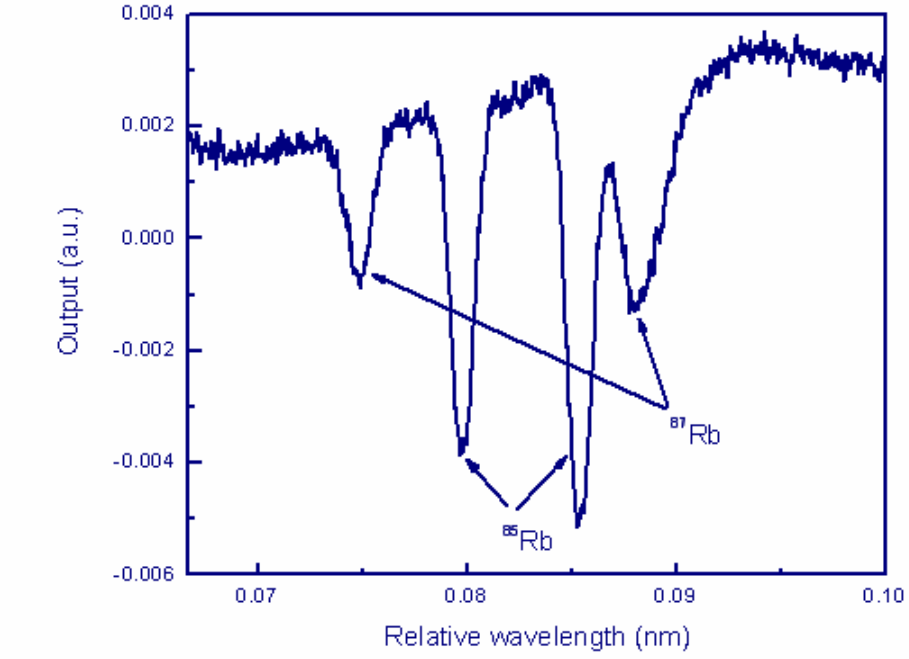

Figure 5. 6 Absorption spectrum from the rubidium vapor filled ARROW.

5.4 Temperature Dependence in ARROW

The temperature dependence of the rubidium absorption in the ARROW's hollow core followed the same trend as the absorption in a bulk cell. Figure 4.7 shows the temperature dependence of rubidium absorption in ARROWs compared to the dependence in a bulk cell. The figures were compiled by first recording absorption spectrums for different temperatures. A single absorption peak was then selected to do the calculations with, the inset in Figure 4.7 shows the peak selected. In this case the peak with the highest frequency near the D_2 transition was selected. For every temperature the far-resonant, I_0, and the on-resonant, I_1, output values were obtained. I_1 and I_0 are related by Equation 1:

$$I_1 = I_0 * \exp(-\alpha * L). \quad (1)$$

In the equation α is the absorption coefficient and L is the ARROW hollow core length. Using Equation 3 and the measured values of I_1 and I_0, α is calculated. Theoretically,

$$\alpha = N * \sigma. \quad (3)$$

In Equation 3, N is the density of rubidium atoms in the cross section and σ is the absorption cross section, which is calculated theoretically. Using, the calculated value of σ and the previously obtained value for α, the density of rubidium atoms in the ARROW is calculated and plotted (Figure 4.7).

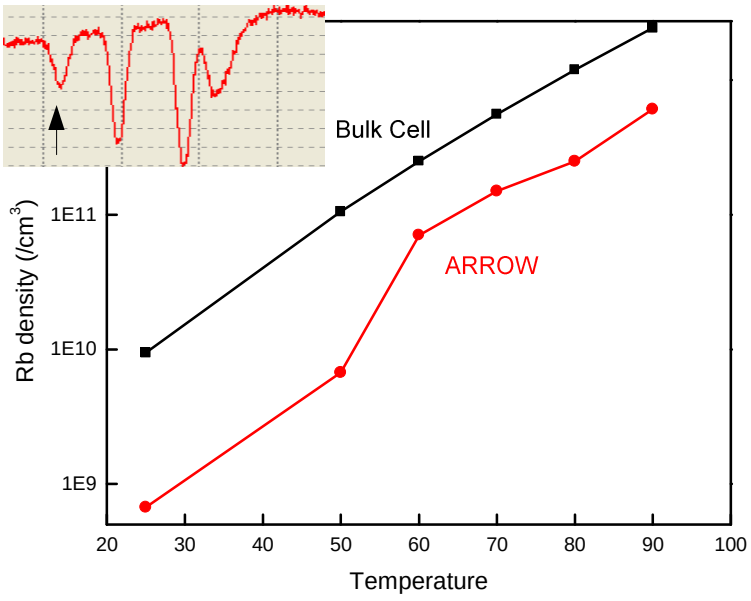

Figure 5. 7 The temperature dependence of rubidium atoms in ARROWs and bulk cells.

High optical densities were measured in the ARROW. Equation 4 shows how the optical density is obtained:

$$OD = \alpha * L. \tag{4}$$

Using the far-resonant, I_0, and the on-resonant, I_1, output values with Equation 1 gives the optical density. For temperatures above 80 C an optically dense medium can be created with optical densities as high as 2.14. With optical densities this high the ARROW device has potential for detecting nonlinear quantum coherence effects [13].

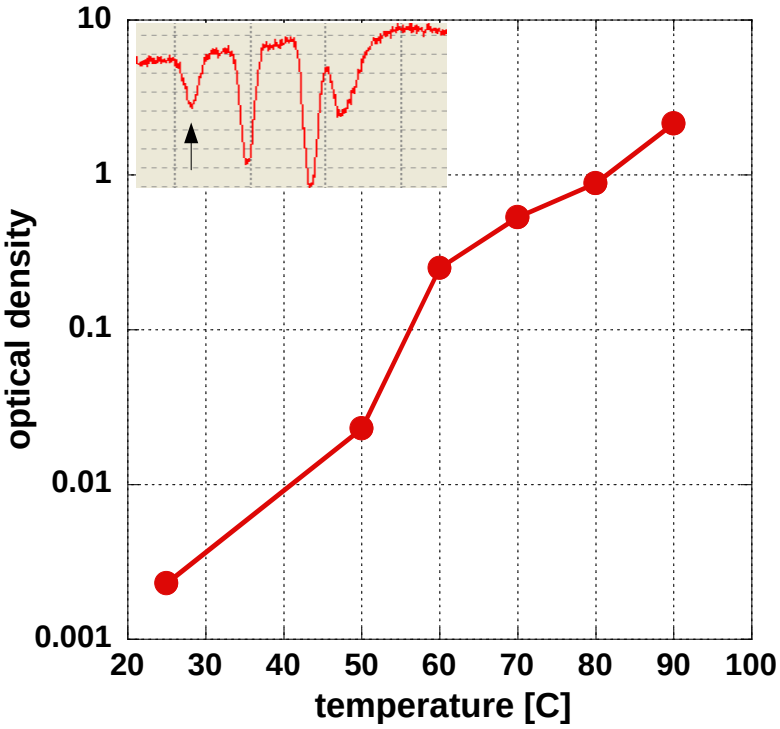

Figure 5. 8 The optical density of rubidium vapor as a function of temperature in an ARROW device.

5.5 Detection of 90 Degree Scattering in ARROW

To show the effective use of the solid core waveguide which intersects the hollow core ARROW a scattering measurement was taken. A probe beam coupled onto the chip into one of the intersecting solid core waveguides. The beam propagated through the solid core waveguide and crossed through the hollow core device. A photodetector detected the output from the solid core waveguide which couples directly into the hollow core waveguide. Light propagating through the hollow core coupled into this solid core waveguide and was detected. The light detected by the photodetector scattered 90 degrees in the ARROW. The output spectrum shows the rubidium absorption dips, showing that

the light did travel through the rubidium-filled hollow core. The intersecting waveguide is essential for use in resonant fluorescence detection, simplified Doppler-free spectroscopy, and parametric generation.

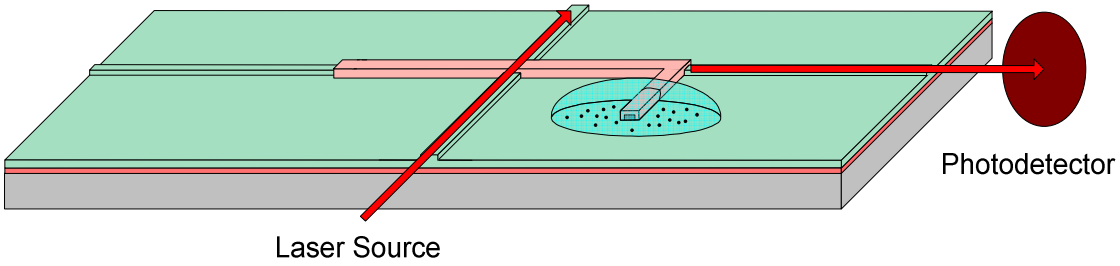

Figure 5. 9 The test setup for the scattering measurement.

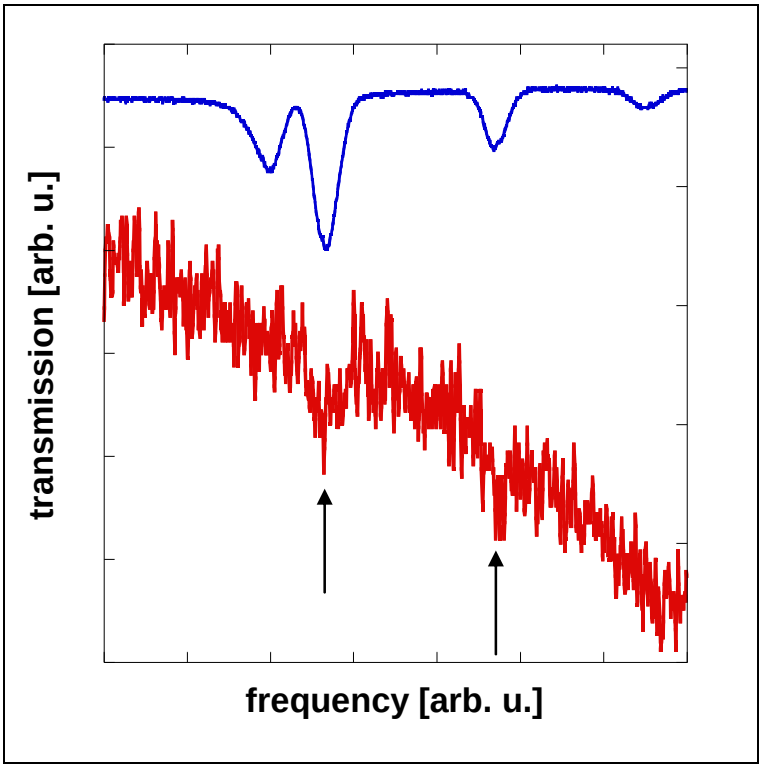

Figure 5. 10 The output spectrum of light which scattered 90 degrees in the ARROW. The rubidium absorption peaks of ^{85}Rb are visible.

5.6 Saturation Absorption Spectroscopy in ARROW

The device for the saturation absorption spectroscopy measurement was fabricated in the same way as the device for the absorption spectroscopy. A stainless steel standoff was modified and epoxied over one of the channel openings of the ARROW. Epoxy placed over the other opening sealed the hollow channel. In the helium filled glovebox rubidium was transferred to the stainless standoff, which was sealed off with a screw and o-ring. A single external cavity diode laser tuned to 780 nm was split into two beams, a pump and a probe beam. The pump beam was approximately twenty times more intense than the probe beam. These beams were coupled onto the chip on opposite sides and propagated in opposite directions through the rubidium vapor filled hollow core (Figure 4.11). This setup follows the typical setup for saturation absorption spectroscopy shown in Figure 1.5 and discussed in Section 1.2.4.

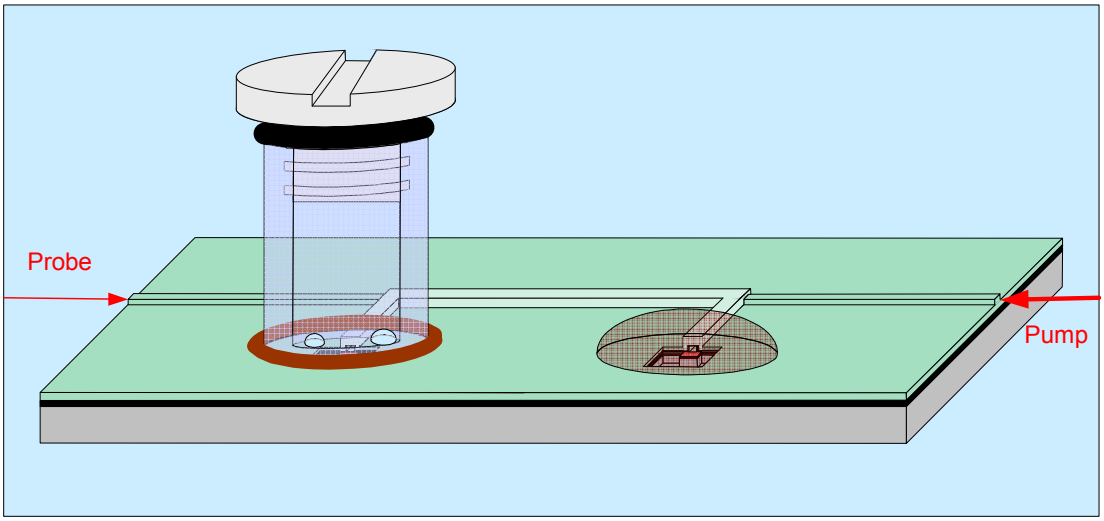

Figure 5. 11 Setup for the saturation absorption spectroscopy easurement.

As expected the more intense pump beam saturated the transitions. The probe beam saw Lamb dips characteristic of saturated absorption spectroscopy. Figure 4.12 shows the absorption of the probe beam as a function of frequency with the pump beam both on and off. When the probe is turned on the Lamb dips are present. The saturated absorption spectrum does not show all of the hyperfine transitions shown in the plot in Figure 1.7. Unfortunately, in the ARROW device most of the Lamb dips were overwhelmed by the absorption peaks.

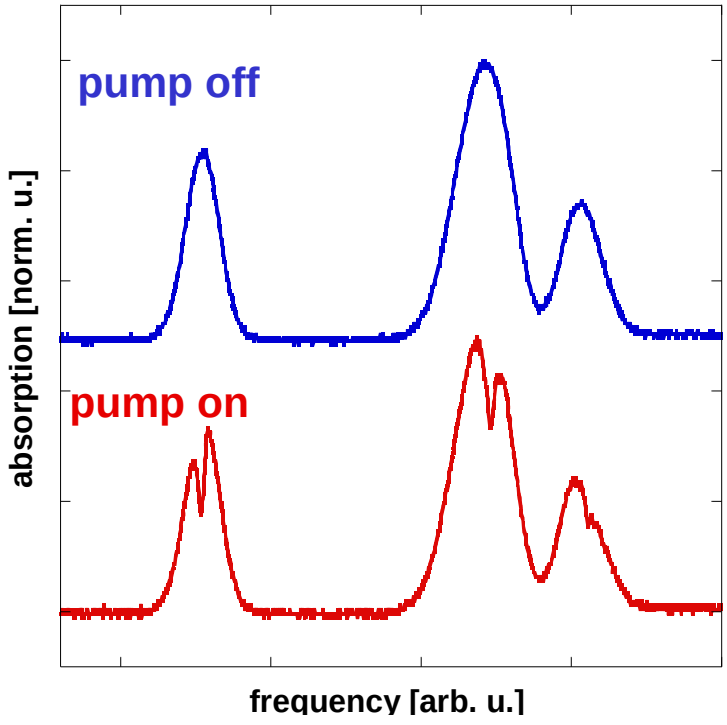

Figure 5. 12 Absorption spectrum with the pump beam turned on and off. When the pump beam is on saturated absorption spectroscopy's characteristic Lamb dips are present.

6 Conclusions

6.1 Summary

Miniaturization and simplification of quantum interference investigation can be accomplished using hollow ARROW waveguide platforms. Using the ability to seal vapor cells onto planar waveguides, rubidium vapor can be integrated into the hollow waveguides. Through experimentation, epoxies were able to seal the atomic vapor cells onto the platform. Further tests showed the effectiveness of rubidium transferring through the length of the waveguide and thus the effectiveness of the channels in containing an atomic vapor. Atomic absorption spectroscopy through the hollow waveguide showed the rubidium absorption peaks around the D_2 line. Further analysis of the absorption peaks revealed a high density of rubidium atoms in the hollow core, which corresponded to a high optical density. Scattering measurements showed the versatility of the planar device setup. Finally, saturated absorption spectroscopy measurements showed the hollow core ARROW was suitable for a common precision spectroscopy application.

6.2 Future Work

Improvement on the ARROW integrated atomic vapor cell platform in the near future will focus on three main areas. The first is finding better self assembling monolayer coatings. No coatings were consciously deposited on the walls of the hollow

cores in the devices fabricated for the absorption measurements. It is believed that the epoxy used to seal the channel and to attach the stainless standoff outgassed and coated the walls. However, this coating failed once the device was heated above 100 C. Other work must be done to decrease the buffer gas pressure in the cell. With the current fabrication technique the buffer gas pressure can not be adjusted. The pressure of the hollow core is equivalent to the pressure in the glovebox when it is sealed. The glovebox is typically kept at a pressure higher than 760 Torr to ensure that oxygen does not leak in. The higher pressure in the core increases broadening of the absorption peaks. Also, the lifetime of the devices is relatively short. New means of sealing the rubidium into the cell will have to be employed to increase the lifetime.

References

[1] S. Knappe, V. Gerginov, P. D. D. Schwindt, V. Shah, H. G. Robinson, L. Hollberg and J. Kitching, "Atomic vapor cells for chip-scale atomic clocks with improved long-term frequency stability," *Opt. Lett.*, vol. 30, pp. 2351, 2005.

[2] F. Benabid, G. Antonopoulos, J. C. Knight and P. St. J. Russell, "Stokes amplification regimes in quasi-cw pumped hydrogen-filled hollow-core photonic crystal fiber," *Phys. Rev. Lett.*, vol. 95, pp. 213903, 2005.

[3] T. W. Hansch, J. Alnis, P. Fendel, M. Fischer, C. Gohle, M. Herrmann, R. Holzwarth, N. Kolachevsky, T. Udem and M. Zimmermann, "Precision spectroscopy of hydrogen and femtosecond laser frequency combs." *Philos. Transact. A Math Phys. Eng. Sci.*, vol. 363, pp. 2155-2163, 2005.

[4] W. Demtroder, *Laser Spectroscopy.*, 3rd ed. Springer, 2003.

[5] A. M. C. Dawes, L. Illing, S. M. Clark and D. J. Gauthier, "All-optical switching in rubidium vapor," *Science*, vol. 308, pp. 672, 2005.

[6] S. E. Harris, "Electromagnetically induced transparency," *Phys. Today*, vol. 50, pp. 36, 1997.

[7] M. D. Lukin, "Colloquium: Trapping and manipulating photon states in atomic ensembles," *Rev. Mod. Phys.*, vol. 75, pp. 457-472, 2003.

[8] L. V. Hau, S. E. Harris, Z. Dutton and C. H. Behrroozi, "Light speed reduction to 17 metres per second in an ultracold atomic gas," *Nature*, vol. 397, pp. 594, 1999.

[9] M. D. Eisaman, A. Andre, F. Massou, M. Fleischhauer, A. S. Zibrov and M. D. Lukin, "Electromagnetically induced transparency with tunable single-photon pulses," *Nature*, vol. 438, pp. 837-841, 2005.

[10] L. Liew, S. Knappe, J. Moreland, H. Robinson, L. Holberg and J. Kitching, "Microfabricated alkali atom vapor cells," *Appl. Phys. Lett.*, vol. 84, pp. 2694, 2004.

[11] H. Schmidt and A. R. Hawkins "Electromagnetically induced transparency in alkali atoms integrated on a semiconductor chip", *Appl. Phys. Lett,* vol. 86, pp. 032106, 2005.

[12] H. Schmidt, D. Yin, W. Yang, D. B. Conkey, J. P. Barber, A. R. Hawkins, B. Wu "Towards Integration of quantum interference in alkali atoms on a chip", *Proceedings of the SPIE* 6130, 2006, pp. 1-11.

[13] W. Yang, D. B. Conkey, R. Brenning, A. R. Hawkins, and H. Schmidt "Atomic Spectroscopy on a Chip", In review *Nature Photonics.*

[14] D. Yin, A. R. Hawkins, and H. Schmidt, "Design of integrated hollow-core waveguides for EIT on a chip," presented *at OSA Annual Meeting,* Tucson, AZ, October 15-20, 2005.

[15] H. Schmidt, D. Yin, W. Yang, D. B. Conkey, J. P. Barber, A. R. Hawkins, "Towards integration of quantum interference in alkali atoms on a chip," SPIE Photonics West, January 23-25, San Jose, CA, 2006.

[16] W. Yang, D. Yin, B. Wu, H. Schmidt, D. B. Conkey, E. J. Lunt, A. R. Hawkins, "Monolithically integrated atomic vapor cell for quantum optics on a chip," 90th OSA Annual Meeting, October 8-12, Rochester, NY, 2006.

[17] D.B. Conkey, R.L. Brenning, A.R. Hawkins, W. Yang, B. Wu, H. Schmidt, "Microfabrication of integrated atomic vapor cells," Photonics West, January 20-25, San Jose, CA, 2007.

[18] H. Schmidt, W. Yang, B. Wu, D. Yin, D. B. Conkey, J. Hulbert, and A. R. Hawkins, "Rubidium spectroscopy on a chip," Invited talk, Photonics West, January 20-25, San Jose, CA, 2007.

[19] J. P. Marangos, "Topical review: Electromagnetically induced transparency," *J. Modern Optics,* vol. 45, pp. 471-503, 1998.

[20] Y. Li and M. Xiao, "Electromagnetically induced transparency in a three-level Λ-type system in rubidium atoms," *Phys. Rev. A,* vol. 51, pp. R2703-R2706, 1995.

[21] M. A. Bouchiat and J. Brossel, "Relaxation of optically pumped Rb atoms on paraffin-coated walls," *Phys. Rev.,* vol. 147, pp. 41-54, 1966.

[22] H. G. Robinson and C. E. Johnson, "Narrow 87Rb hyperfine-structure resonances in an evacuated wall-coated cell," *Appl. Phys. Lett.,* vol. 40, pp. 771-773, 1982.

[23] M. Klein, I. Novikova, D. F. Phillips and R. L. Walsworth, "Slow light in paraffin-coated Rb vapor cells," *J. Modern Optics,* vol. 53, pp. 2583-2591, 2006.

[24] S. Ghosh, J. E. Sharping, D. G. Ouzounov and A. L. Gaeta, "Resonant optical interactions with molecules confined to hollow core photonic band-gap fibers," *Phys. Rev. Lett.,* vol. 94, pp. 093902, 2005.

[25] S. Knappe, V. Velichansky, H. Robinson, L. Liew, J. Moreland, J. Kitching and L. Holberg, "Atomic vapor cells for miniature frequency references," in *2003 IEEE International Frequency Control Symposium and PDA Exhibition Jointly with the 17th European Frequency and Time Forum,* 2003, pp. 31-32.

[26] S. Knappe, P. D. D. Schwindt, V. Gerginov, V. Shah, H. G. Robinson, L. Hollberg and J. Kitching, "Microfabricated atomic clocks and magnetometers," in *Proceeding of the 17th International Conference on Laser Spectroscopy,* 2005, pp. 1-10.

[27] R. Thapa, K. Knabe, M. Faheem, A. Naweed, O. L. Weaver and K. L. Corwin, "Saturated absorption spectroscopy of acetylene gas inside large-core photonic bandgap fiber," *Opt. Lett.,* vol. 31, pp. 2489-2491, 2006.

[28] S. Ghosh, A. R. Bhagwat, C. K. Renshaw, S. Goh and A. L. Gaeta, "Low-light-level optical interactions with rubidium vapor in a photonic band-gap fiber," *Phys. Rev. Lett.,* vol. 97, pp. 023603, 2006.

[29] M. A. Duguay, Y. Kokubun and T. L. Koch, "Antiresonant reflecting optical waveguides in SiO2-Si multilayer structures," *Appl. Phys. Lett.,* vol. 49, pp. 13-15, 1986.

[30] J. P. Barber, "Fabrication of hollow optical waveguides on planar substrates," dissertation, 2006.

[31] J. P. Barber, D. B. Conkey, J. R. Lee, N. B. Hubbard, L. L. Howell, D. Yin, H. Schmidt and A. R. Hawkins, "Fabrication of hollow waveguides with sacrificial aluminum cores," *IEEE Photon. Tech. Lett.,* vol. 17, pp. 363, 2005.

[32] N. B. Hubbard, L. L. Hubbard, J. P. Barber, D. B. Conkey, A. R. Hawkins and H. Schmidt, "Structural models and design rules for on-chip micro-channels with sacrificial cores," *J. Micromech. Microeng.,* vol. 15, pp. 720-727, 2005.

[33] H. Schmidt, D. Yin, J. P. Barber and A. R. Hawkins, "Hollow-core waveguides and 2D waveguide arrays for integrated optics of gases and liquids," *IEEE J. Sel. Top. Quant. Electron.,* vol. 11, pp. 519, 2005.

[34] D. Yin, J. P. Barber, E. J. Lunt, A. R. Hawkins and H. Schmidt, "Optical characterization of arch-shaped ARROW waveguides with liquid cores," *Optics Express,* vol. 13, pp. 10566-10570, 2005.

[35] J. P. Barber, E. J. Lunt, Z. A. George, D. Yin, H. Schmidt and A. R. Hawkins, "Integrated hollow waveguides with arch-shaped cores," *IEEE Photon. Tech. Lett.,* vol. 18, pp. 28-30, 2006.

[36] D. Yin, J. P. Barber, A. R. Hawkins and H. Schmidt, "Waveguide loss optimization in hollow-core ARROW waveguides," *Optics Express*, vol. 13, pp. 9331-9336, 2005.

[37] S. Briaudeau, D. Bloch and M. Ducloy, "Sub-Doppler spectroscopy in a thin film of resonant vapor," *Phys. Rev. A*, vol. 59, pp. 3723-3735, 1999.

[38] J. C. Camparo, "Alkali <I-S> wall relaxation in dichlorodimethylsilane coated resonance cells," *J. Chem. Phys.*, vol. 88, pp. 1533-1539, 1987.

[39] C. R. Kessel and S. Granick, "Formation and Characterization of a Highly Ordered and Well-Anchored Alkylsilane Monolayer on Mica by Self-Assembly," *Langmuir*, vol. 7, pp. 532-538, 1991.

APPENDIX

APPENDIX A Process Flow

This appendix describes the general process for fabrication of hollow ARROW waveguides. The optional step includes a raised silicon pedestal etch before waveguide formation. The bulk of this flow comes from John Barber. More information on the ARROW fabrication process can be found in his dissertation [30].

1) (Optional) Pedestal process:
    a. Pattern SU8 using the pedestal etch mask with a target thickness of 10 μm.
    b. Oxygen plasma descum for 90 seconds.
    c. Perform an RIE silicon etch using CF_4 gas in the Anelva DEM-451 machine for 50 minutes.
    d. Perform a 5 minute oxygen plasma descum.
    e. Remove SU-8 residue in Nano-Strip at 90°C for 60 minutes, followed by a DI water rinse.
    f. Measure pedestal height and width using the profilometer. If incorrect, scrap the wafer and start over, adjusting the etch time as needed. The correct height should be equal to the total thickness of all PECVD deposited top layers.
2) Remove native oxide in HF or buffered oxide etch (BOE), 1 minute or until the wafer dewets, followed by a DI water rinse.
3) Bottom dielectric layer deposition:

a. Clean and season both PECVD chambers for the appropriate film type.
b. Place a bare silicon test wafer in the PECVD chamber and deposit a test film (1 minute, 45 second deposition for oxide, 10 minute deposition for nitride).
c. Measure the test wafer using the ellipsometer and calculate the film growth rate.
d. For nitride, adjust the refractive index of the film by changing the ammonia (NH_3) flow rate. An increased ammonia flow lowers the refractive index. Run more test wafers as necessary to achieve the desired refractive index.
e. Place the wafer in the PECVD chamber and deposit the desired film using the measured growth rate from above to calculate the correct deposition time.
f. Blow particles off of the wafer with a nitrogen gun and perform an SC-1 clean to remove remaining particles.
g. Repeat steps a through f for each required dielectric layer.

4) Deposit and pattern the sacrificial core using the appropriate process for SU-8.
5) Perform a 1 minute oxygen plasma descum.
6) Deposit the upper dielectric layers using the process in step 4 above, but omit the SC-1 clean between layers.
7) Solid-core waveguide formation:
    a. Pattern SU-8 with a target thickness of 5 μm using the appropriate mask.
    b. Perform a 1 minute oxygen plasma descum.

c. Perform an RIE oxide etch in the Anelva DEM-451 for 9 minutes.

8) Core expose etch:
    a. Do a 2 minute oxygen plasma descum followed by a Nano-Strip etch at 90°C for 30 minutes and a DI water rinse.
    b. Pattern SU-8 with a target thickness of 10 μm using the appropriate mask.
    c. Perform a 1 minute oxygen plasma descum.
    d. Perform an RIE oxide etch in the Anelva DEM-451 for 45 minutes.
    e. Perform a 5 minute oxygen plasma descum.
9) Place wafer in Nano-Strip etchant to remove the sacrificial core material
    a. Hotplate temperature should be 90°C for Nano-Strip
    b. Nano-Strip should be replaced every 24-48 hours with fresh solution. Care must be taken during the core removal etch to avoid breaking the waveguides. Slowly siphon off the old acid without disturbing the wafer.
10) Carefully remove the etchant from the beaker and rinse the waveguides with DI water 6 times by slowly adding water, gently agitating, and draining the water. After rinsing, soak the pieces in DI water for 24 hours, followed by 2 more DI water rinses. Dry the waveguides by placing the beaker on a hotplate at 90°C for 30 minutes or until the remaining water has evaporated.
11) Inspect the waveguides using a microscope and cleave as desired.

APPENDIX B ARROW Designs

The ARROW designs presented in this appendix are specifically designed for air-core ARROWs where the index of the core is 1. Occasionally the design must be redesigned because of new PECVD growth conformalities. The PECVDs have different growth rates in the vertical and horizontal directions. Conformality is measured as a ratio between the vertical growth rate and the horizontal growth rate. The two older designs (Tables B.3 and B.4) were designed for an oxide conformality of 1.4. The newer designs (Tables B.1 and B.2) have a conformality of 1.32.

Table B. 1 The ARROW design for a pedestal ARROW with oxide conformality 1.32.

Specifications		Layer Structure	
		Layer	Thickness (nm)
Wavelength	780 nm	Oxide 6	3020
Core	Air	Nitride 6	100
Core Shape	Rectangle	Oxide 5	140
Nitride Index	2.10	Nitride 5	260
		Oxide 4	220
Conformality (Vertical : Horizontal)		Nitride 4	270
Nitride	1.2	Core	5 μm
Oxide	1.32	Nitride 3	106
Pedestal		Oxide 3	548
		Nitride 2	106
		Oxide 2	548
Designed February 2007		Nitride 1	106
		Oxide 1	548
		Substrate	-

Table B. 2 The ARROW design for a regular ARROW with oxide conformality 1.32.

Specifications		Layer Structure	
		Layer	Thickness (nm)
Wavelength	780 nm	Oxide 6	3040
Core	Air	Nitride 6	392
Core Shape	Rectangle	Oxide 5	308
Nitride Index	2.10	Nitride 5	120
		Oxide 4	216
Conformality (Vertical : Horizontal)		Nitride 4	250
Nitride	1.2	Core	5 µm
Oxide	1.32	1.2	106
Regular		1.32	548
		Nitride 2	106
		Oxide 2	548
Designed February 2007		Nitride 1	106
		Oxide 1	548
		Substrate	-

Table B. 3 The ARROW design for a pedestal ARROW with oxide conformality 1.4.

Specifications		Layer Structure	
		Layer	Thickness (nm)
Wavelength	780 nm	Oxide 6	4178
Core	Air	Nitride 6	90
Core Shape	Rectangle	Oxide 5	124
Nitride Index	2.10	Nitride 5	134
		Oxide 4	110
Conformality (Vertical : Horizontal)		Nitride 4	352
Nitride	1.2	Core	5.8 µm
Oxide	1.4	Nitride 3	111
Pedestal		Oxide 3	546
		Nitride 2	111
		Oxide 2	546
Designed January 2006		Nitride 1	111
		Oxide 1	546
		Substrate	-

Table B. 4 The ARROW design for a regular ARROW with oxide conformality 1.4.

Specifications		Layer Structure	
		Layer	Thickness (nm)
Wavelength	780 nm	Oxide 6	3402
Core	Air	Nitride 6	139
Core Shape	Rectangle	Oxide 5	379
Nitride Index	2.10	Nitride 5	162
		Oxide 4	216
Conformality (Vertical : Horizontal)		Nitride 4	303
Nitride	1.2	Core	5.8 μm
Oxide	1.4	Nitride 3	110
Regular		Oxide 3	550
		Nitride 2	110
		Oxide 2	550
Designed January 2006		Nitride 1	110
		Oxide 1	550
		Substrate	-

APPENDIX C Publications

Archival Journal Publications

1. W. Yang, D. B. Conkey, R. Brenning, A. R. Hawkins, and H. Schmidt, “Atomic Spectroscopy on a Chip”, In review *Nature Photonics*

2. H. Schmidt, D. Yin, W. Yang, D. B. Conkey, J. P. Barber, A. R. Hawkins, B. Wu, "Towards Integration of quantum interference in alkali atoms on a chip", *Proceedings of the SPIE* 6130, pp. 1-11, 2006.

3. B. A. Peeni, D. B. Conkey, J. P. Barber, R. Kelly, M. L. Lee, A. T. Wooley, and A. R. Hawkins, "Planar Thin Film Device for Capillary Electrophoresis", *Lab on a Chip,* vol. 5, pp.501-505, 2005.

4. N.B. Hubbard, L.L. Howell, J.P. Barber, D.B. Conkey, A.R. Hawkins, and H. Schmidt, "Mechanical models and design rules for on-chip micro-channels with sacrificial cores", *J. of Micromech. Microeng.,* vol. 15, pp. 720-727, 2005.

5. J.P. Barber, D.B. Conkey, J.R. Lee, N.B. Hubbard, L.L. Howell, H. Schmidt, and A.R. Hawkins, "Fabrication of Hollow Waveguides with Sacrificial Aluminum Cores,” *IEEE Phot. Tech. Lett., vol 17*, pp. 363-365, 2005.

Conference Publications

1. D.B. Conkey, R.L. Brenning, A.R. Hawkins, W. Yang, B. Wu, H. Schmidt, "Microfabrication of integrated atomic vapor cells," Photonics West, January 20-25, San Jose, CA, 2007.

2. H. Schmidt, W. Yang, B. Wu, D. Yin, D.B. Conkey, J. Hulbert, and A.R. Hawkins, "Rubidium spectroscopy on a chip", Invited talk, Photonics West Conference, San Jose, CA, Jan 21-25, 2007.

3. W. Yang, D. Yin, B. Wu, H. Schmidt, D. B. Conkey, E. J. Lunt, A. R. Hawkins, "Monolithically Integrated Atomic Vapor Cell for Quantum Optics on a Chip," 90th OSA Annual Meeting, October 8-12, Rochester, NY, 2006.

4. H. Schmidt, D. Yin, W. Yang, D. B. Conkey, J. P. Barber, A. R. Hawkins, "Towards integration of quantum interference in alkali atoms on a chip," SPIE Photonics West, January 23-25, San Jose, CA, 2006.

5. J. P. Barber, D. B. Conkey, M. M. Smith, J. R. Lee, B. A. Peeni, Z. A. George, A. R. Hawkins, D. Yin, and H. Schmidt, "Hollow waveguides on planar substrates with selectable geometry cores," Conference on Lasers and Electro-Optics/International QUantum Electronics Conference, May 22-25, Baltimore, MD, 2005.

6. B. A. Peeni, D. B. Conkey, A. T. Woolley, M. L. Lee, and A. R. Hawkins, "Electro-osmotic Pumps Constructed Using Sacrificial Etching," 28th International Symposium on Capillary Chromatography and Electrophoresis, May 22-25, Las Vegas, NV, 2005.